Lawrence Berkeley National Laboratory

Recent Work

Title

HIGH-SPIN ROTATIONAL STATES IN 169Hf FROM THE 159Tb (14N, 4ny) REACTION AND DECAY OF 169Ta

Permalink

https://escholarship.org/uc/item/3sm8b92q

Authors

Rezanka, I.
Ladenbauer-Bellis, I.M.
Rasmussen, J.O.
et al.

Publication Date

1975-01-26

eScholarship.org Powered by the California Digital Library
University of California

Submitted to Physical Review C

LBL-2965
(Yale 3076-15)
Preprint

HIGH-SPIN ROTATIONAL STATES IN ^{169}Hf FROM THE ^{159}Tb (^{14}N, 4nγ) REACTION AND DECAY OF ^{169}Ta

I. Rezanka, I. M. Ladenbauer-Bellis, J. O. Rasmussen, W. Ribbe, and E. der Mateosian

January 26, 1975

RECEIVED
LAWRENCE
RADIATION LABORATORY

FEB 25 1975

LIBRARY AND
DOCUMENTS SECTION

Prepared for the U. S. Atomic Energy Commission
under Contract W-7405-ENG-48

TWO-WEEK LOAN COPY

This is a Library Circulating Copy which may be borrowed for two weeks. For a personal retention copy, call Tech. Info. Division, Ext. 5545

LAWRENCE BERKELEY LABORATORY
UNIVERSITY OF CALIFORNIA

LBL-2965

DISCLAIMER

This document was prepared as an account of work sponsored by the United States Government. While this document is believed to contain correct information, neither the United States Government nor any agency thereof, nor the Regents of the University of California, nor any of their employees, makes any warranty, express or implied, or assumes any legal responsibility for the accuracy, completeness, or usefulness of any information, apparatus, product, or process disclosed, or represents that its use would not infringe privately owned rights. Reference herein to any specific commercial product, process, or service by its trade name, trademark, manufacturer, or otherwise, does not necessarily constitute or imply its endorsement, recommendation, or favoring by the United States Government or any agency thereof, or the Regents of the University of California. The views and opinions of authors expressed herein do not necessarily state or reflect those of the United States Government or any agency thereof or the Regents of the University of California.

LBL-2965

HIGH-SPIN ROTATIONAL STATES IN ^{169}Hf FROM THE ^{159}Tb (^{14}N, 4nγ) REACTION AND DECAY OF ^{169}Ta*

I. Rezanka† and I. M. Ladenbauer-Bellis

Heavy Ion Accelerator Laboratory
Yale University
New Haven, Connecticut 06520

and

J. O. Rasmussen and W. Ribbe‡

Nuclear Chemistry Division
Lawrence Berkeley Laboratory
University of California
Berkeley, California 94720

and

E. der Mateosian

Physics Division
Brookhaven National Laboratory
Upton, New York 11973

January 1975

ABSTRACT

The high-spin levels of the deformed nucleus ^{169}Hf were studied by γ-ray spectroscopy, both in-beam following the heavy-ion reaction ^{159}Tb(^{14}N, 4nγ)^{169}Hf and out-of-beam from β decay of ^{169}Ta. The half-life of ^{169}Ta was remeasured as 4.7 ± 0.7 m. Three rotational bands were assigned in ^{169}Hf: $5/2^-[523]$ ground band, up to spin 31/2; $5/2^-[512]$, 59.1 keV band head, up to spin 15/2; and $5/2^+[642]$, $7/2^+$ band head at 28.80 keV, up to spin 41/2 and tentatively up to spin 49/2. The $7/2^+$ band head of the $5/2^+[642]$ band is isomeric and decays with a half-life of 82^{+40}_{-15} ns to the ground state. The g-factors in the negative parity bands were deduced from the measured angular distributions and branching ratios and compared to the predictions of the Nilsson model. Both this test and the systematics of the moments of inertia confirm the proposed assignments. The $5/2^+[642]$ band (originating in the 13/2 shell-model state) is strongly perturbed. This band does not backbend although the ^{168}Hf core does at a lower rotational angular momentum than attained in ^{169}Hf. The consequence of this observation for the explanation of backbending is discussed. The mixing amplitudes in the positive parity band are compared with the predictions of Pyatov's theory.

[NUCLEAR REACTIONS ^{159}Tb (^{14}N, 4nγ)^{169}Hf, E = 56-92 MeV; measured E_γ, I_γ (θ), γγ coin, $T_{1/2}$ of 28.80 keV level. ^{169}Hf deduced levels, J, π, K, g, $\frac{\hbar^2}{2\mathcal{J}}$
RADIOACTIVITY ^{169}Ta; measured $T_{1/2}$, E_γ, I_γ ^{169}Hf deduced levels, J, π, K.]

I. INTRODUCTION

Studies of nuclear high-spin rotational states have led in recent years to the discovery of two new effects: sudden changes of the moment of inertia at high rotational velocities (backbending),[1,2] and the weakening of the coupling of the last odd particle to the core in unique parity states.[3,4] A complete understanding of both effects has not yet been achieved; both may be, in fact, related to Coriolis effects.[5] To arrive at a more definitive theoretical explanation, further experimental measurements are needed. The experimental studies should probably stress two directions: studying the nuclear high spin states in new nuclear species, and extending the knowledge about already investigated nuclei to even higher spin states. This study of ^{169}Hf has followed both lines.

The experimental work on this project was done as a cooperative effort of Yale, Berkeley, and Brookhaven National Laboratory groups. The first experiments on this study were made at the Yale Heavy Ion Accelerator (HIA) where both the decay of ^{169}Ta and the excitation function of ^{169}Hf in the ^{159}Tb (^{14}N, 4n) reaction were studied. Following this preliminary in-beam spectroscopy, the final experiments on $\gamma\gamma$-coincidences and angular distributions were done at the Brookhaven Laboratory tandem van de Graaf.

II. EXPERIMENTAL PROCEDURES AND RESULTS

A. Decay of ^{169}Ta

1. Beam and targets

The beam of ^{16}O from HIA was used in this investigation to bombard a 99.9% pure metallic Tb foil. The foil was rolled manually to a thickness of 3-4 mg/cm^2. The energy of the ^{16}O ions, accelerated originally to 10.4

MeV/AMU, was adjusted by means of Aℓ degrading foils placed immediately in front of the Tb target. Two Tb foils were irradiated in one target assembly consisting of Aℓ degraders, Tb foils, and a water-cooled backing, all in physical contact. Only the second Tb foil (downstream in the beam) was used for the measurements to avoid counting of the radioactive recoils, from the Aℓ foils, implanted into the next foil in the beam direction. The energy of the beam reaching the target was 116 MeV. Control runs were performed also at lower and higher energies to assure the optimum production of ^{169}Ta. The duration of irradiation was 5 m.

2. Isolation of Ta activity

Chemical isolation of Ta activity from the Tb target material was accomplished by a method similar to that described by Felber.[6] The irradiated target was dissolved in hot 6 N HCl, and the rare earth fluorides were precipitated by using 2-3 drops of concentrated HF. The mixture was centrifuged and the supernatant solution was transferred to a separatory funnel where 3 ml of di-isopropylketone was used to extract the Ta activities. This solution was then used as the source for the γ- and X-ray spectroscopy. The time elapsed between the end of the bombardment and the beginning of the measurement was 3-5 m.

3. Gamma-ray spectra

The γ-ray spectra were measured by means of a Ge(Li) detector (volume 40 cm^3, resolution 2.1 keV at 1332 keV) in several time intervals for each sample. For a particular series of measurements, these intervals were kept equal within feasible limits for several samples, and the spectra were added together. The resulting spectra were then analyzed by a non-linear

least squares program SAMPO,[7] which was also used for all spectrum analyses reported in this study. The energy calibration obtained for stronger peaks from a simultaneous measurement with calibration standards is believed to be accurate to 0.1 keV for these stronger peaks. Both the time dependence of line intensities and the excitation functions were used for the assignment to ^{169}Ta; for the latter, the prominent γ transitions excited in the decay of the well known[8,9] 3.25 m daughter product ^{169}Hf served as an indication of the presence of ^{169}Ta. From these measurements, the half-life of ^{169}Ta was remeasured and found to be equal to 4.7±0.7 m, in agreement with the value 5.0 m reported by the Dubna group.[10] In addition to these measurements, several ^{169}Ta samples contained in thin-walled plastic bottles were counted by means of a Si(Li) detector. The detector used was 3 mm deep and 10 mm in diameter; the resolution was 200 eV at 5.6 keV. A spectrum obtained in this experiment is shown in Fig. 1. The accuracy of energy determination of the very low energy lines is believed to be ± 40 eV; for the energy region of X-rays and above, the accuracy is about ± 100 eV. The intensities were related to the intensities of higher energy lines by normalizing to the overlapping portions of both spectra.

The information on the transitions in the decay of ^{169}Ta obtained from these γ-ray experiments is summarized in Table I. The errors in energy determination are 0.1 keV unless stated otherwise. In the same table the errors of the intensities are 10% for lines stronger than 50 units and 20% for the rest.

4. Partial decay scheme of ^{169}Ta

Although the scope of the experimental information on ^{169}Ta decay obtained in this study does not permit construction of a complete decay scheme, a partial decay scheme, including several low-lying levels of ^{169}Hf bearing a special significance for the in-beam studies described later in

this work, could be proposed. The ^{169}Hf ground state is almost certainly the $5/2^-[523]$ Nilsson orbital. Both the β-decay[8,9] of this ground state to the levels in ^{169}Lu, and the systematics of the 97-neutron nuclei[11] are strong arguments for such an assignment. The 77.7 keV and 177.0 keV transitions appear to belong to the rotational band built on this orbital, depopulating the first and second excited levels of this band, respectively. The moment of inertia of this band in ^{169}Hf agrees well with the values of the moment of inertia of $5/2^-[523]$ bands found in other 97 neutron nuclei (see Table II).

In the low-energy part of the spectrum, the most striking feature is the very intense 28.8 keV line. Considering the low energy, and consequently strong internal conversion of this γ line, it can be shown that it must contain an appreciable E1 component. First, we note the KX group of Hf. Due to the selected beam energy, irradiation and counting times, the X rays mainly decay with the half-life of ^{169}Ta and must originate partially from ^{169}Ta electron capture, partially in the internal conversion in ^{169}Hf, and partially in other Hf nuclei The intensities of the two well resolved KX lines, $K_{\alpha 1}$, and $K_{\beta 2}$, corrected both for the known ratios to the remaining components of the Hf KX group[13] and for the fluorescence yield,[14] have an intensity of 2,800 in the units of Table I. This value (total number of K vacancies in Hf atoms of all possible origins) is certainly the upper limit of the intensity of ^{169}Ta decays via electron capture. Adding to this number one-half of the intensity of the annihilation radiation (630), the upper limit of 3,430 for the intensity of ^{169}Ta decay is obtained. From comparison in Table III, of this limiting value with the intensities of the 28.8 keV transition for different assumptions about its multipolarity, the conclusion about a significant E1 component in this

transition follows. In addition, such a strong transition must directly populate the ground state, since no other gammas of comparable strength are observed. Similar but less conclusive arguments can be used for the 38.2 keV transition. In this case, it is felt that there exists only a preference and not a rigorous proof for the E1 assignment.

Based on these considerations, a partial decay scheme for ^{169}Ta (Fig. 2) is proposed. The 99.3 keV, $9/2^- \rightarrow 7/2^-$ transition was obviously masked by the $2^+ \rightarrow 0^+$ transition in ^{170}Hf, always present in our spectra.

B. Reaction ^{159}Tb (^{14}N, 4nγ)^{169}Hf

1. Beams and targets

As in the ^{169}Ta decay study, metallic self-supporting Tb targets were used for the in-beam studies. The Tb was rolled into foils 2-7 mg/cm^2 thick. The thickness of the target was chosen from this range according to the requirements of a particular experiment. In order to avoid the growth of an oxide layer on the surface, new targets were prepared for each experiment.

The beam of ^{14}N from HIA was used in the first part of this study. The energy of the beam was varied by means of degrading foils positioned at the intermediate beam focus between the two analyzing magnets. The ^{14}N beam was also used in the final experiments at the BNL Tandem, where only one of the two MP Tandem accelerators was used.

2. Excitation functions

A preliminary experiment consisting of several single γ-ray runs were performed at Yale HIA. The same 40 cm^3 Ge(Li) detector, as was used for the ^{169}Ta study, was used for this experiment. The energy of the ^{14}N beam was varied from 56 to 92 MeV with a 2.1 mg cm^{-2} thick target.

By comparing the increasing, and then decreasing, intensities of the known gamma transitions[16,17] in the adjacent doubly-even ^{168}Hf and ^{170}Hf, the transitions with maximum relative intensities lying between the maxima for the ^{170}Hf and ^{168}Hf were assigned to the ^{169}Hf nucleus. The optimum ^{14}N beam energy for the population of ^{169}Hf was found to be 70 MeV. Because of the low duty cycle (2%) of the HIA, this procedure was applicable only to the strong transitions above 100 keV, with relative intensities exceeding 40 in the units of Table IV. The γ lines which were assigned in this way to ^{169}Hf have the isotopic assignments in Table IV (column 6) underlined.

3. Search for millisecond isomers

The time structure of Yale HIA (beam on for 2 ms, beam off for 98 ms) was exploited in the search for the existence of isomeric states in ^{169}Hf with half-lives in the ms region. The γ-ray spectra were collected repeatedly from various time intervals following the beam burst. No such isomeric states were observed, and it was concluded that the upper limit for population by the ^{159}Tb (14N, 4nγ) ^{169}Hf reaction, of an isomeric state in ^{169}Hf, with a half-life in the range 50 ns - 200 ms and decaying by γ-ray emission, is 0.1% of the total population of ^{169}Hf nuclides.

An additional value of the Yale HIA experiments with the 2% duty cycle was the discrimination of γ-rays from induced radioactivity. Thus, we could distinguish in the 100% duty cycle BNL spectra the radiations due to the radioactivity produced in the Tb target from the prompt γ-rays from the nuclear reaction.

4. Singles γ-ray spectra

During the γγ-coincidence experiments at BNL described in detail in section 6, a singles γ-ray spectrum was counted by means of a 60 cm^3 Ge(Li) detector having a resolution of 1.5 keV at 662 keV. The spectrum is shown in Fig. 3. In addition to the energy calibrations taken before, after, and several times during the run, the γγ-coincidence experiment was followed by the simultaneous counting of the γ-rays from the reaction and from the radioactive standards: ^{133}Ba, ^{182}Ta, and ^{22}Na. The efficiency calibration of the detector was obtained by counting several radioactive sources with accurately known decay schemes. A careful computer analysis by the code SAMPO[7] made it possible to resolve many close multiplets of the spectrum. The results are summarized in Table IV; the energies are believed to be accurate to 0.1 keV unless explicitly stated. The intensities of column 2 of Table IV are considered good to 10% for the well resolved lines with intensities above 10 units and 20% for the rest. In a few instances, the intensities of weak lines are missing altogether; these lines were observed only in the coincidence spectra.

5. Angular distributions

The angular distribution experiment was performed at the BNL Tandem. The ^{14}N beam with the incident energy of 71 MeV was used for the irradiation of a 7 mg cm^{-2} thick Tb target. The thicker target and consequently higher incident beam energy than for the maximum production of ^{169}Hf with a thinner target were chosen in order to minimize the recoil into vacuum of the reaction products. In addition to the detector described in 4, another Ge(Li) detector with a resolution of 2.0 keV at 662 keV and 40 cm^3 active volume was used.

The detectors were positioned 8 cm from the beam spot on the target; the position of the smaller one was kept stationary, at 36^{o} to the beam direction while the larger detector was attached to a support moving through eight discrete angles with respect to the beam, between 30^{o} and 120^{o}. The experiment was performed under the control of a SIGMA-7 computer. The spectra from the movable detector were repeatedly collected at the different angles with the spectrum corresponding to each angle being stored separately in the memory. The counting for one angle in each series lasted about 10 m. A window closely covering the 218.6 keV line of the spectrum in the stationary detector was counted simultaneously, both directly (with a negligible dead time correction), and subjected to the dead time influence of the first detector. The counts in the stationary detector served both for the dead time correction and the normalization of the spectra at different angles. The resulting spectra were first analyzed by means of the computer code SAMPO,[7] and then the normalized γ-ray intensities obtained by analysis were fitted by a least squares method to the formula

$$A(\theta) = A_o + A_2 P_2 (\cos\theta) + A_4 P_4 (\cos\theta) \quad . \qquad (1)$$

The results of these fits for A_2 and A_4 are shown in columns 3 and 4 of Table IV, respectively, together with the standard deviations.

6. Gamma-Gamma coincidences

The ^{14}N beam energy was decreased to 67 MeV, and Tb targets 1.8 - 2.2 mg/cm^2 thick were used throughout this run. The lower energy of the beam, slightly below the optimum for the population of ^{169}Hf, caused a pronounced decrease in the population of ^{168}Hf. In order to prevent the build-up of

long-lived activities, the target was replaced every 8 hours. The same detectors as were used for the angular distribution measurements (5), namely, with volumes 60 and 40 cm^3, were used also for the $\gamma\gamma$ coincidence run. The detectors were positioned perpendicular to the beam direction, on the opposite sides of the beam line and at a distance of 2 cm from the beam spot on the target. A standard fast-slow coincidence system was used; the timing signal of the smaller, 40 cm^3 detector was obtained by using the Constant Fraction Timing Discriminator (Ortec model 463), while the Extrapolated Zero Strobe (Canberra model 1426) was used with the 60 cm^3 detector. The energy ranges were 10-2000 keV for the former, 30-2000 keV for the latter detector; a timing efficiency close to 100% was achieved only at about 80 keV and above in the latter case. For this dynamic range, the timing resolution obtained with the ^{22}Na source was 25 ns, and in the actual run when the low energy component was very intense, the resolution changed to 50 ns. The digitized information about coincident events including the pulse heights in each of the two detectors and the time between the detection of the quanta, was recorded serially on a magnetic tape and sorted following the completion of the experiment. The range of the time-to-amplitude converter was set at 400 ns.

The summary of the coincidence relations revealed by this experiment is given in the Table V. All established coincidences were prompt, with strong maxima contained within 50 ns of the prompt peak. The only exceptions were the coincidences obtained with the STOP signal derived from the 28.8 keV line. Although the experiment was not originally intended for this purpose, it turned out to be possible to obtain an approximate value for the half-life of the level depopulated by the 28.8 keV transition. The time spectra used

for this purpose are shown in Fig. 4. The open circles were obtained from those events which corresponded to quanta with energies above 108 keV in the START detector, and to the net full-energy peak of the 28.8 keV line in the STOP detector; the solid dots, representing the "prompt" curve under these specific conditions, corresponds to the same energy range in the START detector but to the portions of the continuum immediately adjacent, on both sides, to the 28.8 keV peak in the STOP detector. In spite of low statistics the delayed character of the 28.8 keV transition is apparent. The value of 81 ns for this half life was obtained manually by the slope method and the value of 84 ns by the method of moments; the resulting value $82\ ^{+40}_{-15}$ ns adopted, while the quoted uncertainties include both statistical and possible systematic errors. When reversing the energy selection in the two detectors, curves essentially symmetrical with those of Fig. 4 were obtained, but a smaller number of time channels available for the delayed spectrum precluded a quantitative comparison.

When the cascades of strong coincident γ rays were established, more subtle results of this experiment were brought out by adding together the coincident spectra with gates on several of the transitions in the cascade. An example of this procedure is shown in Fig. 5 for the two strong cascades in ^{169}Hf, one ending by the 218.6 keV transition, the other having the 166.5 and 207.1 keV γ lines at the bottom of the cascade. The results of this analysis are shown in Table VI.

7. Levels in ^{169}Hf

Although all data described in the preceding sections are important for the level assignment and interpretation, the results of the coincidence experiment provided the most direct information about the rotational bands in ^{169}Hf. The

coincidence results formed the main basis for the assignment of all rotational levels resulting from this study.

The three lowest levels of the $5/2^-[523]$ rotational band were already assigned from the ^{169}Ta decay. Here, in the in-beam study, this band was also observed and identified up to considerably higher excitations. It was found that it consisted of two cascades with weak cross-feeding. The only $\Delta I = -1$ transitions positively observed here, are the two lowest ones; otherwise, only the $\Delta I = -2$ stretched transitions formed the band up to spins 31/2 and 29/2.

The two strong cascades shown in Fig. 5 are obvious candidates for the decoupled positive parity band occurring regularly in odd-neutron rare earth nuclei.[18] This assignment follows both from their spacing and from their population patterns. The delayed coincidences of both cascades with the 28.8 keV, E1 transition ending in the ground state prove this assignment. Although such a band is a Coriolis mixture of several Nilsson orbitals originating in the $i_{13/2}$ shell-model state, and the perturbation may be effective even for low rotational excitations, the prevailing single particle character for the low excitations should be $5/2^+[642]$. The spacings and intensities in the stronger of the cascades show, for example, that the 218.6 keV γ-line is the $17/2^+ \rightarrow 13/2^+$ transition; this, and the angular distributions enable us to assign this band starting with the $9/2^+$ level and extending reliably to spin 41/2 and tentatively to 49/2. However, such direct coincidence information was missing for the level structure at very low rotational excitation below $9/2^+$. To resolve this problem two experimental results were used: 1) The I + 1/2 ODD cascade in the $5/2^-[523]$ ground band was in coincidence with a weak 148.4 keV transition, and there was an energy fit within 0.1 keV between the sum of

this transition with the 28.80 keV one, and the 177.1 keV excitation of the $9/2^-$ state. 2) A marginally visible coincidence of the 207.1 keV transition populating the $11/2^+$ state of the [642] band, and the 73.2 keV transition was noticed. In addition to the stronger decay of the $11/2^+$ level to the $9/2^+$ level via the 67.4 keV transition, this 73.2 transition was interpreted as a $\Delta I = -2$ decay to the $7/2^+$ level. Both points 1 and 2 led to the assignment of the 28.8 keV level as the $7/2^+$ band head of the $5/2^+[642]$ band. This means also that, very tentatively, the $5/2^+$ member of this band would lie at 38.2 keV. Both the inversion of the spin sequence, and the proximity of three low-spin levels can be well understood in terms of Coriolis perturbation of this band.

In addition to these two bands, a third band was observed in this work, having its band head at 59.1 keV and decaying via three interband transitions to the ground state. The assignment of this band presented a problem: one would expect the $3/2^-[521]$ Nilsson state to be close to the Fermi level, and this band would be a choice for such an assignment, but the moment-of-inertia is in sharp disagreement with the value regularly found for this band in the neighboring nuclei,[11] and in particular, in ^{165}Yb.[19] Although the occurrence of the $5/2^-[512]$ state so close to the $5/2^-[523]$ ground state is surprising and certainly not predicted by the Nilsson scheme, the g-factors found within this band, discussed later in the paper (Section III.A.1), led to this assignment for the third band. The level scheme of ^{169}Hf resulting from this study is shown in Fig. 6.

III. DISCUSSION

A. Negative parity bands

1. Energy Spectra

The two negative-parity bands observed in this work, $5/2^-[523]$ and $5/2^-[512]$ were fitted by the rotational formula[20,21]

$$E_{rot} = A\{I(I+1)-K^2\} + B\{I(I+1)-K^2\}^2 + \cdots + (-1)^{I+K} \prod_{i=I-K}^{K} (I+i)$$

$$\{A_{2K} + \cdots\} \quad . \qquad (2)$$

The least squares fit is shown in Fig. 7 for the $5/2^-[523]$ band. A very noticeable Coriolis perturbation of the band is apparent; this perturbation is very much present at the very bottom of the band, and this is the region where the formula (2), in which the Coriolis interaction was included only in the perturbational approach,[21] gives a relatively poor fit. It seems quite possible that Coriolis interaction with an unobserved higher-lying $3/2^-$ band accounts for the somewhat surprising proximity of these two $5/2^-$ bands.

The resulting rotational parameters of the two negative parity bands are summarized in Table VII. The rotational parameter

$$A = \hbar^2/2\mathcal{J} \quad , \qquad (3)$$

for the $5/2^-[512]$ band is included in the systematics shown in Fig. 8. Here, the rotational parameters A of this band [11,23,24] are plotted both in the N = 97 and Z = 72 sections of the N, Z plane. A good fit of this $5/2^-$ excited band in ^{169}Hf with the systematic behavior of this band in the neighboring nuclei is evident.

2. Nuclear g-factors

Fundamental information can be obtained from the E2/M1 mixing amplitudes δ. In addition, in reference back to Section II. B.7, this analysis is even more important for the reassurance of the assignment of the $5/2^-[512]$ band. Information of two kinds is available for this purpose: The results of

the angular-distribution measurements, and the cross-over to cascade branching ratios within the band. Generally the branching ratios yield more accurate absolute values of δ but cannot determine the sign, and the reliability hinges on the validity of the strong coupling model. The angular distributions determine the sign of δ unequivocally and its absolute value usually rather inaccurately, both in a model-independent way.

The determination of the mixing amplitude in the ground band turned out to be difficult; the cascade transitions were very weak and were only observed for the two lowest excited levels of the band. Moreover, the only usable case, the $9/2^- \rightarrow 7/2^-$, 99.3 keV transition was not resolved in the singles spectrum from the transition in the other $5/2^-$ band, and was close to the 100.3^- keV, $2 \rightarrow 0$ transition in ^{170}Hf. Fortunately, the I(99.3)/I(177.1) branching ratio could be reliably determined from the γ spectrum coincident with the cascade feeding the $9/2^-$ level, and was found equal to 0.15. From this value, the absolute value of δ was determined and is shown in Table VIII. The angular distribution results were combined with the branching ratios to obtain the mixing amplitudes for the $5/2^-[512]$ band, given also in Table VIII.

The mixing amplitude is directly related to the nuclear g-factor by the relation[25]

$$g_K - g_R = \frac{Q_o E_\gamma}{1.073\ (I^2 - 1)^{\frac{1}{2}}} \frac{1}{\delta} \quad , \qquad (4)$$

where Q_o is the nuclear quadrupole moment in barns, E_γ the energy of the cascade transition in MeV, and I the initial spin. The value of 5.5 barns was taken for the value of Q_o, extrapolated from the tabulated B(E2) values

of heavier Hf nuclei[26] according to the A-dependence of the 2 → 0 transitions in the doubly-even nuclei. The results of this determination are given in column 6 of Table VIII, and in column 7 they are compared with the calculated[27] values. For that purpose, the value of 0.30 was used for g_R. The agreement appears to be good.

Returning to the choice between the assignments of $5/2^-[512]$ or $3/2^-[521]$ single-particle character to the second **negative** parity band, the mixing amplitudes and g-factors were also determined for this band under the alternate assumption about its single-particle character and compared to the mentioned[27] Nilsson scheme values in Fig. 9 for both assignments. The agreement with the predicted values, in the case of the $5/2^-[512]$, and disagreement in the case of the $3/2^-[521]$ assignment is apparent. Thus, the assigned single-particle character of the $5/2^-[512]$ band is confirmed.

B. Positive parity band

1. Moment of inertia

The doubly-even core of ^{169}Hf would correspond to the ^{168}Hf nucleus. This doubly-even nucleus was found to backbend[17] at spin 14. It is therefore extremely interesting to test the dependence of the moment-of-inertia of ^{169}Hf on the rotational velocity of the core. In contrast to the doubly-even nuclei where the first order relation of the nuclear rotation to the total nuclear angular momentum is obvious and the only possible questions arise about higher order "curvature" effects,[16] the separation of the nuclear rotation from other contributions in an odd nucleus is not simple. What is more serious, the separation is dependent on the model which should itself be tested by this analysis. An acceptable solution is to use an approximation,

in the comparison of ^{169}Hf and ^{168}Hf, which gives the minimum possible rotational velocity ω at a given spin. If this is done, and the states with the same ω are then compared, one can be sure that the rotational velocity in the odd-mass case is not lower than in the corresponding doubly-even case. The model which can be used in this case for the positive parity bands exists and was proposed earlier by Vogel.[28] In the extreme first approximation of this model, the yrast branch of the band is the result of the stretched coupling of the rotation with the single-particle motion

$$I = R + j \quad , \tag{5}$$

and j in this case is 13/2. Under this assumption, the backbending, if the inertial properties of the core are not influenced by the last odd neutron, should occur at spin $41/2^+$ of the $5/2^+[642]$ band. It can be seen from Fig. 10 where the comparison with ^{168}Hf is displayed, that the $5/2^+[642]$ band does not backbend. It should be emphasized that the nature of the approximation used for obtaining R for the positive parity band in ^{169}Hf is such that, in better approximation, the curve could be only shifted to the higher R. On the same sample, the $5/2^-[523]$ band is also shown; the relation[29]

$$R^2 = I(I+1) - K^2 \quad , \tag{6}$$

was used here.

This observation can be interpreted as favoring Stephens' and Simon's explanation[5] of backbending. If indeed the decoupled $i_{13/2}$ two-neutron band is responsible for the backbending in the ^{168}Hf, one would not expect the band in ^{169}Hf based on the $i_{13/2}$ neutron to backbend. On the contrary, the

mixing with the three-neutron states of the same shell-model character should be strong, and the moment-of-inertia would change only gradually in the 5/2[642] band, as is observed here. Clearly, experiments on other nuclei are needed to obtain a more generally valid evidence for this effect.

2. Mixing amplitudes

The mixing amplitudes δ can be determined for several $\Delta I = -1$ transitions of the positive parity band. As shown in Fig. 11 for the 15/2 to 13/2 transition, the experimental value of A_2 of Eq. (1) is such that after correction for the real population of magnetic states, as obtained by using the pure E2 transition from the same level, the corrected A_2 indicates maximum constructive interference for the asymmetry of the angular distribution and gives δ near $-0.8 \pm .1$. The analysis for the $\Delta I = -1$ transition from the $19/2^+$ and $23/2^+$ states is similar but we attach greater uncertainty ± 0.5 to the δ values of about -1.0, that is a 50:50 mixture of M1 and E2 photon radiation. With the δ values we proceed to calculate the following ratios of $B(E2; I \rightarrow I-2)/B(E2; I \rightarrow I-1)$: for I = 15/2, 1.01; for I = 19/2, $\sim$ 3.7; and for I = 23/2, $\sim$ 8.6. These ratios deviate strongly from the Alaga branching rules for any given K value, the first value (I = 15/2) lying half way between Alaga values for K = 5/2 and K = 7/2, the second value near K = 5/2, and the third between K = 3/2 and K = 5/2. Pyatov and collaborators[30] have made detailed calculations of such deviations from Alaga branching ratios for Coriolis-mixed bands, and though they obtain trends of deviations in the same direction as our results, their deviation shifts in no case are nearly as large as our experimental value.

It is appropriate to compare the positive parity band in ^{169}Hf with those of ^{161,163,165}Er as determined by Hjorth et al.[3] In general spacing and in the bunching into doublet structure the ^{169}Hf band most closely resembles ^{163}Er,

especially for spins greater than 13/2. Their theoretical cross-over to cascade gamma intensity ratios exhibit the large increase with spin shown by our data, though the disagreement with their own Er data is often a factor of two or so. The discussion[31] of the weakness of the $15/2^+$ to $13/2^+$ "unfavored" E2 transition in ^{155}Dy is also relevant here. Neither our own Coriolis band mixed wave functions[31] nor those of ref. 30 gave enough cancellation to match the experimental weakness of the $\Delta I = -1$ transition. Evidently Coriolis mixing (i.e., the approach to the decoupled band limit) occurs more rapidly with increasing spin than is given by most Coriolis band mixing calculations. Perhaps the attenuation factor invoked for off-diagonal Coriolis matrix elements increases rapidly toward unity for increasing spin. There is no universally accepted explanation of the attenuation factor, so it is not clear just how to revise the theory to reproduce the branching behavior and band energies in ^{169}Hf.

The negative sign of δ in the positive parity band indicates a negative $g_K$eff, consistent with the $i_{13/2}$ quasi-particle character. However, a quantitative calculation of g values is not feasible in view of the failure of Alaga branching rules for the E2 components and in view of the lack of level lifetime information.

The pure E2 cross-over transitions of both the positive parity band and the $5/2^-$[523] show strong positive anisotropies. The high degree of spin alignment thus implied indicates most feeding coming through a cascade of stretched transitions.

IV. ACKNOWLEDGMENTS

The authors wish to thank Dr. W. B. Jones for making the Si(Li) detector available for this study. The generous cooperation of the Brookhaven Tandem Laboratory staff is most appreciated. During the course of this study, W. Ribbe has received support of the Hahn-Meitner Institute in West Berlin. J. O. Rasmussen wishes to acknowledge support of a J. S. Guggenheim fellowship in 1973.

FOOTNOTES AND REFERENCES

*Work performed under the auspices of the U. S. Atomic Energy Commission.

†Present address: Xerox Corporation, Rochester, New York.

‡Present address: Städt Rudolf-Virkchow Krankenhaus, Strahlungsabteilung, 1 Berlin 65.

1. A. Johnson, H. Ryde, and J. Starkier, Phys. Letters 34B, 605 (1971).
2. A. Johnson, H. Ryde, and S. A. Hjorth, Nucl. Phys. A179, 753 (1972).
3. S. A. Hjorth, H. Ryde, K. A. Hageman, G. Løvhøiden, and J. C. Waddington, Nucl. Phys. A144, 513 (1970).
4. I. Rezanka, F. M. Bernthal, J. O. Rasmussen, R . Stokstad, I. Fraser, J. Greenberg, and D. A. Bromley, Nucl. Phys. A179, 51 (1972).
5. F. S. Stephens and R. S. Simon, Nucl. Phys. A183, 257 (1972).
6. F. F. Felber, Jr., University of California Report No. UCRL-3618, 1957 (unpublished).
7. J. T. Routti and S. G. Prussin, Nucl, Instr. Methods 72, 125 (1969).
8. Y. Y. Chu and J. Reednick, Phys. Rev. C2, 310 (1970).
9. B. J. Meijer, F. W. N. deBoer, and P. F. A. Goudsmit, Nucl. Phys. A204, 636 (1973).
10. R. Arlt, A. Malek, G. Muziol, and H. Strunsy, Izv. Akad. Nauk SSSR, Ser. Fiz. 33, 1266 (1969).
11. M. E. Bunker and C. W. Reich, Rev. Mod. Phys. 43, 348 (1971).
12. A. A. Abdurazakov, K. Ya. Gromov, V. Zvolská, T. Islamov, and H. Strusny, Izv. Akad. Nauk SSR, Ser. Fiz. 35, 698 (1971).

13. C. M. Lederer, J. M. Hollander, and I. Perlman, Table of Isotopes (J. Wiley, New York, 1967), p. 570.

14. I. Bergström and C. Nordling in Alpha-, Beta-, and Gamma-Ray Spectroscopy, K. Siegbahn ed. (North-Holland. Amsterdam, 1965), p. 1534.

15. R. S. Hager and E. C. Seltzer, Nucl. Data A4, 1 (1968).

16. Ø. Saethre, S. A. Hjorth, A. Johnson, S. Jägare, H. Ryde, and Z. Symanski, Nucl. Phys. A207, 486 (1973).

17. R. M. Lieder, H. Beuscher, W. F. Davidson, A. Neskakis, and C. Mayer-Boricke, Proc. Int. Conf. on Nuclear Physics, J. deBoer and J. G. Mang ed. (Munich, 1973), (North-Holland Publishing Co.) p. 188.

18. F. S. Stephens. P. Kleinheinz, R. K. Sheline, and R. S. Simon, Nucl. Phys. A222, 235 (1974).

19. L. L. Riedinger, P. H. Stelson, E. Eichler, D. C. Hensley, N. R. Johnson, R. L. Robinson, R. O. Sayer, G. J. Smith, and G. B. Hageman, Proc. Int. Conf. on Reactions between Complex Nuclei (North-Holland, Amsterdam, 1974), p. 175, and private communication.

20. I. Hamamoto and T. Udagawa, Nucl. Phys. A126, 291 (1969).

21. A. Bohr and B. R. Mottelson, Monograph on Nuclear Structure, to be published.

22. A. Kerman, Dan. Mat. Fys. Medd. 30 No. 15 (1956).

23. S. Hultberg, I. Rezanka, and H. Ryde, Nucl. Phys. A205, 321 (1973).

24. I. Rezanka, J. O. Rasmussen, F. M. Bernthal, C. T. Alonso, J. R. Alonso, S. Hultberg, and H. Ryde, Nucl. Phys. A179, 430 (1972).

25. F. Boehm, G. Goldring, G. B. Hagemann, G. D. Symons, and A. Tveter, Phys. Letters 22, 627 (1966).

26. P. H. Stelson and L. Grodzins, Nucl. Data A1, 21 (1965).

27. I.-L. Lamm, Nucl. Phys. A125, 504 (1969).

28. P. Vogel, Phys. Letters 33B, 400 (1971).

29. S. A. Hjorth, H. Ryde, and B. Skånberg, J. de Physique 33, 23 (1972).

30. M. I. Baznat, N. I. Pyatov, and M. I. Chernej, Phys. Scripta 6, 227 (1972); M. I. Baznat, M. I. Chernej, and N. I. Pyatov, "Polarization Effects in the Rotational Motion of Odd-Mass Nuclei", II, JINR Report E4-5550 (1970) and III, JINR Report E4-6265, Dubna, USSR (1972).

31. K. Krien, R. A. Naumann, J. O. Rasmussen, and I. Rezanka, Nucl. Phys. A209, 572 (1973).

Table I. Gamma Rays in the ^{169}Ta Decay

E_γ (keV)	I_γ (arb. units)
28.80 ± 0.04	230
38.18 ± 0.04	57
55.81 ± 0.06[a]	1,350
65.1[b]	125
68.5[c]	38
77.7[c]	16
132.8	20
153.5	80
170.4[c]	18
177.0	24
187.8 ± 0.2	12
192.4	100[d]
230.0	28
394.5	35
404.0 ± 0.2	21
440.8	38
511.0[c]	1,260
520.4 ± 0.2	20
529.0 ± 0.2	26
547.4 ± 0.3	20
595.0 ± 0.2	59

[a] Hf $K_{\alpha 1}$. [b] Hf $K_{\beta 2}$. [c] Isotopic assignment uncertain.

[d] Adopted value.

Table II. Values of $\hbar^2/2\mathcal{J}$ for the rotational band built on the $5/2^-[523]$ orbital in nuclei with 97 neutrons.

Nucleus	$^{161}_{64}Gd_{97}$	$^{163}_{66}Dy_{97}$	$^{165}_{68}Er_{97}$	$^{167}_{70}Yb_{97}$	$^{169}_{72}Hf_{97}$
$\hbar^2/2\mathcal{J}$ (keV)	10.4[a]	10.5[a]	11.0[a]	11.2[b]	11.1[c]

[a] Ref. 11.

[b] Ref. 12.

[c] This work.

Table III. Comparison of the 28.8 keV transition intensity (total) with the ^{169}Ta decay intensity.

	^{169}Ta decay	28.8 keV		
		E1	E2	M1
I_{tot} (arb. units)	$\leqslant$ 3,430[a]	700[b]	250,000	6,400

[a] See text for the deduction of this value.

[b] Internal conversion coefficients interpolated from tables by Hager and Seltzer (Ref. 15) were used to compute these values.

Table IV. Summary of γ Radiations Produced in Tb Target by ^{14}N Beam

E_γ (keV)	Photon Intensity $I_\gamma(90°)$ (Arb. units)	Angular Distribution Coefficient A_2/A_o	A_4/A_o	Photon Intensity Corrected for Anisotropy[a] (Arb. units)	Assignments nucleus	band	levels
22.0±0.2	54						
23.1	260						
26.1	45						
28.8	150				^{169}Hf		$5/2^+ \rightarrow 5/2^-$
32.1	710						
33.2±0.2	120						
34.2	350						
54.3	1020				Hf $K_{\alpha 2}$		
					Lu $K_{\alpha 1}$		
55.9	450				Hf $K_{\alpha 1}$		
58.1±0.2	1500				^{159}Tb	$3/2^+[411]$	$5/2 \rightarrow 3/2$
59.1					^{169}Hf		$5/2^- \rightarrow 5/2^-$
61.3	220						
63.1	190				Hf $K_{\beta 1}$		
65.1	60				Hf $K_{\beta 2}$		
67.3	30				^{169}Hf	$5/2^+[642]$	$11/2 \rightarrow 9/2$
68.6	17				^{169}Hf	$5/2^+[642]$	$11/2 \rightarrow 7/2$
73.2±0.2	17						
75.0	23						
76.4±0.2	25						

(continued)

Table IV. cont.

E_γ (keV)	$I_\gamma 90^o$ (Arb. units)	Angular Distribution Coefficient A_2/A_o	A_4/A_o	I_γ (Arb. units)	Assignments nucleus	band	levels
77.8	53	+0.32±0.21	+0.09±0.31	63	^{169}Hf	$5/2^-[523]$	7/2 → 5/2
79.5	1060	-0.02±0.04	+0.06±0.07	1050	^{159}Tb	$3/2^+$	7/2 → 5/2
84.8	15						
86.4	45	+0.01±0.16	+0.12±0.23	45	^{160}Dy	0^+	2 → 0
87.4	56	+0.19±0.16	+0.04±0.23	62	^{168}Yb	0^+	2 → 0
88.5	43						
92.9±0.2	9	-0.08±0.32	+0.31±0.45	9			
94.5	23						
99.6	29	-0.19±0.11	+0.14±0.16	26	^{169}Hf ^{169}Hf	$5/2^-[523]$ $5/2^-[512]$	9/2 → 7/2 7/2 → 5/2
100.8	27	+0.08±0.08	-0.09±0.12	28	^{170}Hf	0^+	2 → 0
102.4	29	+0.69±0.22	+0.09±0.30	44	^{166}Yb	0^+	2 → 0
103.9	240	-0.08±0.02	+0.05±0.05	231	^{159}Tb	$3/2^+[411]$	9/2 → 7/2
107.8	41	+0.34±0.04	+0.03±0.07	49	^{169}Hf	$5/2^+[642]$	13/2 → 9/2
111.3±0.2	3						
113.4	9	+0.13±0.17	+0.30±0.28	10			
117.3	7	+0.32±0.20	+0.36±0.30	8			
119.9±0.2	18	+0.18±0.45	+0.61±0.64	20			
121.1	140	-0.01±0.06	+0.02±0.09	140	^{159}Tb	$3/2^+[411]$	11/2 → 9/2
122.3±0.2	24						
123.7	99	+0.23±0.27 +0.00±0.15	+0.46±0.39 -0.21±0.21		^{168}Hf ^{169}Hf	0^+ radioactivity	2 → 0

(continued)

Table IV. cont.

E_γ (keV)	I_γ (Arb. units)	Angular Distribution Coefficient 90°		I_γ (Arb. units)	Assignments		
		A_2/A_o	A_4/A_o		nucleus	band	levels
125.5±0.2	9.4	-0.16±0.21	-0.01±0.30	9			
130.0	29	-0.40±0.08	+0.11±0.13	24	^{169}Hf	$5/2^-[512]$	$9/2 \rightarrow 7/2$
133.4	3.3	+0.08±0.19	+0.14±0.28	3			
137.5	165	-0.16±0.03	+0.07±0.05	153	^{159}Tb	$3/2^+[411]$	$7/2 \rightarrow 3/2$
139.6	6.6	+0.33±0.22	+0.27±0.32	7.9			
146.8	35.1	-0.17±0.07	+0.09±0.12	32			
148.4	50.4	-0.13±0.04	+0.02±0.08	47	^{169}Hf		$9/2^- \rightarrow 7/2^+$
					^{159}Tb	$3/2^+[411]$	$13/2 \rightarrow 11/2$
152.5	7.3	+0.35±0.58	+0.89±0.83	9			
154.1	22.8	-0.47±0.14	-0.11±0.21	18	^{169}Hf	$5/2^-[512]$	$11/2 \rightarrow 9/2$
157.2	9.2	+0.27±0.14	+0.39±0.22	10.6			
158.9	12.1	+0.17±0.20	+0.41±0.30	13	^{169}Hf		$7/2^- \rightarrow 5/2^-$
					^{159}Tb	$3/2^+[411]$	$15/2 \rightarrow 13/2$
162.7	4.8						
164.8	33.5	-0.69±0.16	-0.30±0.25	25			
166.5	111.5	-0.88±0.04	+0.12±0.08	77	^{169}Hf	$5/2^+[642]$	$15/2 \rightarrow 13/2$
169.3±0.2	6.8						
170.8±0.2	7.3						
172.0±0.4	3.2						
177.1	44.0	+0.17±0.06	-0.06±0.10	48	^{169}Hf	$5/2^-[523]$	$9/2 \rightarrow 5/2$
179.3	24.8	-0.32±0.11	0.00±0.17	21	^{169}Hf	$5/2^-[512]$	$13/2 \rightarrow 11/2$
182.0	21.8	+0.13±0.20	+0.17±0.30	23			

(continued)

Table IV. cont.

E_γ (keV)	I_γ 90^o (Arb. units)	Angular Distribution Coefficient A_2/A_o	A_4/A_o	I_γ (Arb. units)	Assignments nucleus	bands	levels
183.4	93.1	-0.03±0.07	+0.05±0.13	92	^{159}Tb	$3/2^+[411]$	$9/2 \rightarrow 5/2$
184.4	34.1	-0.21±0.34	-0.09±0.48	31	^{159}Tb		
187.9±0.3	6.1	0.00±0.27	+0.70±0.40	6			
189.0±0.2	6.0	-0.14±0.34	-0.45±0.50	6			
191.2	21.2	+0.37±0.20	+0.63±0.30	26			
192.7	13.7	+0.09±0.11	+0.21±0.18	14			
197.0	84.9	+0.08±0.03	+0.03±0.05	88	^{160}Dy	0^+	$4 \rightarrow 2$
198.3	51.4	+0.13±0.06	+0.24±0.10	55	^{169}Hf ^{168}Yb	$5/2^-[512]$ 0^+	$15/2 \rightarrow 13/2$ $4 \rightarrow 2$
207.1	100.0	+0.28±0.02	-0.02±0.05	116	^{169}Hf	$5/2^+[642]$	$15/2 \rightarrow 11/2$
210.8±0.2	2.9	+0.38±0.30	+0.13±0.43	3.6	^{159}Tb		$5/2^+ \rightarrow 7/2^+$
213.8±0.2	15.2	-0.46±0.19	-0.27±0.27	12			
216.9±0.2	12.1	+0.12±0.17	+0.20±0.26	13			
218.6	241	+0.26±0.02	-0.07±0.05	277	^{169}Hf	$5/2^+[642]$	$17/2 \rightarrow 13/2$
220.9	94.3	+0.25±0.03	-0.07±0.06	108	^{170}Hf	0^+	$4 \rightarrow 2$
223.3±0.3	19.7	+0.55±0.28	+0.01±0.39	27			
225.0	122	+0.08±0.02	+0.01±0.05	127	^{169}Hf ^{159}Tb	$5/2^-[523]$ $3/2^+[411]$	$11/2 \rightarrow 7/2$ $11/2 \rightarrow 7/2$

(continued)

Table IV. cont.

E_γ (keV)	I_γ 90^o (Arb. units)	Angular Distribution Coefficient A_2/A_o	A_4/A_o	I_γ (Arb. units)	Assignments nucleus	bands	levels
227.9	41.1	+0.03±0.05	-0.05±0.08	42	^{166}Yb	0^+	4 → 2
229.3±0.3	17.4	+0.18±0.18	-0.14±0.26	19	^{169}Yb	$5/2^-$[512]	9/2 → 5/2
238.6	18.1	+0.78±0.19	+0.73±0.27	30			
240.6	6.9	-0.16±0.28	-0.57±0.41	6			
241.9±0.2	6.9						
243.2±0.2	9.1	-0.03±0.26	-0.24±0.37	9			
246.9±0.2	4.2						
249.5±0.2	4.7						
261.7	46.3	+0.21±0.02	-0.02±0.05	52	^{168}Hf	0^+	4 → 2
265.0	16.0	-0.19±0.17	-0.07±0.26	15			
267.1	62.3	+0.30±0.04	0.00±0.07	73	^{169}Hf	$5/2^-$[523]	13/2 → 9/2
269.4	17.6	+0.01±0.06	+0.09±0.10	18	^{159}Tb	$3/2^+$[411]	13/2 → 9/2
270.5±0.2	8.2						
273.8±0.2	3.1	-0.02±0.26	+0.21±0.38	3	^{159}Tb		$1/2^{(-)} \rightarrow 1/2^+$
278.5	47	-0.81±0.07	+0.25±0.11	33	^{169}Hf	$5/2^+$[642]	19/2 → 17/2
284.1	13	+0.26±0.13	0.00±0.21	15	^{169}Hf	$5/2^-$[512]	11/2 → 7/2

(continued)

Table IV. cont.

E_γ (keV)	I_γ 90° (Arb. units)	Angular Distribution Coefficient A_2/A_o	A_4/A_o	I_γ (Arb. units)	Assignments nucleus	bands	levels
288.5±0.2	5.1				^{169}Hf		$9/2^- \rightarrow 5/2^-$
290.5±0.3	3.2				^{159}Tb		$5/2^+ \rightarrow 5/2^+$
295.5±0.2	10						
297.2±0.2	32	+0.10±0.07	+0.05±0.12	34	^{160}Dy	0^+	$6 \rightarrow 4$
298.7±0.2	23	+0.25±0.12	+0.15±0.18	26	^{168}Yb	0^+	$6 \rightarrow 4$
304.6	5.5						
307.1	6.5	+0.13±0.27	+0.07±0.39	7	^{159}Tb	$3/2^+[411]$	$15/2 \rightarrow 11/2$
311.2	47	+0.21±0.04	-0.09±0.07	53	^{169}Hf	$5/2^-[523]$	$15/2 \rightarrow 11/2$
316.1±0.2	16	+0.21±0.21	+0.47±0.31	17			
320.7	88	+0.25±0.06	-0.02±0.10	101	^{170}Hf	0^+	$6 \rightarrow 4$
326.3	194	+0.29±0.02	-0.07±0.05	227	^{169}Hf	$5/2^+[642]$	$21/2 \rightarrow 17/2$
330.8	132	+0.19±0.02	-0.02±0.05	146	^{169}Hf	$5/2^+[642]$	$19/2 \rightarrow 15/2$
333.4±0.4	20	+0.22±0.12	+0.37±0.17	22	^{169}Hf	$5/2^-[512]$	$13/2 \rightarrow 9/2$
337.5	27	+0.23±0.08	0.00±0.13	31	^{166}Yb	0^+	$6 \rightarrow 4$
339.0±0.2	10	-0.18±0.13	+0.09±0.20	9			
340.0±0.2	9.3			8			
346.2	67	+0.29±0.04	-0.05±0.07	78	^{169}Hf	$5/2^-[523]$	$17/2 \rightarrow 13/2$
347.6±0.2	20	-0.11±0.14	+0.26±0.21	19	^{159}Tb		$5/2^+ \rightarrow 3/2^+$
348.7±0.2	19			18			
350.7±0.2	19	-0.49±0.13	+0.65±0.20	15			
352.0±0.2	24	+0.45±0.29	+1.06±0.42	31			

(continued)

Table IV. cont.

E_γ (keV)	I_γ 90^o (Arb. units)	Angular Distribution Coefficient A_2/A_o	A_4/A_o	I_γ (Arb. units)	Assignments nucleus	bands	levels
354.4±0.2	6.8						
363.4	24	0.00±0.09	+0.17±0.14	24	^{159}Tb		$5/2^- \rightarrow 3/2^+$
367.0±0.3	9.7	+0.22±0.21	+0.05±0.31	11			
369.4	117	+0.01±0.04	+0.02±0.07	117	^{169}Hf	radioactivity	
371.2±0.2	26	+0.18±0.02	-0.03±0.05	28	^{168}Hf ^{159}Tb	0^+	$6 \rightarrow 4$ $7/2^+ \rightarrow 5/2^+$
377.6	15	+0.41±0.10	-0.13±0.15	19	^{169}Hf	$5/2^-[512]$	$15/2 \rightarrow 11/2$
379.6±0.2	6.1	+0.09±0.27	+0.07±0.39	6			
381.2±0.2	14.3	+0.72±0.37	-0.20±0.51	22			
383.6±0.3	17.9						
384.5±0.2	36.2	+0.29±0.07	+0.02±0.11	42	^{169}Hf ^{168}Yb	$5/2^-[523]$ 0^+	$19/2 \rightarrow 15/2$ $8 \rightarrow 6$
386.2±0.2	13.4	-0.35±0.20	-0.59±0.29	11	(^{160}Dy	0^+	$8 \rightarrow 6$)
387.8±0.2	7.7						
389.5±0.2	17.9						
390.3±0.2	17.1	-0.94±0.17	+0.17±0.24	11.6	^{169}Hf	$5/2^+[642]$	$23/2 \rightarrow 21/2$
392.3±0.3	7.9	+0.31±0.33	+0.10±0.47	9.3			
394.9±0.3	3.0						
400.3	70	+0.27±0.03	-0.02±0.05	81	^{170}Hf	0^+	$8 \rightarrow 6$
406.3	13.3	+0.33±0.12	-0.13±0.19	16			
411.2	51.8	+0.25±0.08	+0.07±0.13	59	^{169}Hf	$5/2^-[523]$	$21/2 \rightarrow 17/2$
415.0±0.4	2.6						
416.2±1.0	2.1						
423.4	129	+0.29±0.03	-0.08±0.05	51	^{169}Hf	$5/2^+[642]$	$25/2 \rightarrow 21/2$

(continued)

Table IV. cont.

E_γ (keV)	I_γ 90° (Arb. units)	Angular Distribution Coefficient A_2/A_o	A_4/A_o	I_γ (Arb. units)	Assignments nucleus	bands	levels
430.1	17.6	+0.31±0.11	-0.07±0.16	21	^{166}Yb	0^+	8 → 6
436.1±0.3	13	+0.17±0.26	+0.02±0.38	14			
437.9	77.2	+0.26±0.04	-0.10±0.06	89	^{169}Hf	$5/2^+[642]$	23/2 → 19/2
439.9±0.2	10.1	-0.07±0.15	+0.41±0.22	10			
442.0±0.2	12.4	+0.14±0.22	+0.18±0.32	13			
443.5±0.2	15.9	+0.12±0.13	-0.04±0.19	17			
445.2	42.5	+0.26±0.06	+0.01±0.09	49	^{169}Hf	$5/2^-[523]$	23/2 → 19/2
456.8	21.0	+0.25±0.05	-0.08±0.08	24	^{168}Hf	0^+	8 → 6
458.6±0.2	11.2						
460.6	48.2	+0.26±0.05	-0.05±0.08	55	^{169}Hf	$5/2^-[523]$	25/2 → 21/2
462.1	57.7	+0.24±0.05	-0.06±0.08	66	^{170}Hf	0^+	10 → 8
					^{160}Dy	0^+	10 → 8
463.1±0.2	15.8						
468.4	8.5	-0.30±0.20	+0.39±0.30	7.4			
470.5±0.2	5.0	+0.41±0.17	-0.01±0.25	6.3			
475.5±0.3	8.3	+0.38±0.15	+0.13±0.22	10.2			
478.8±0.2	12.8	-0.31±0.16	+0.18±0.23	11.1			
482.1±0.4		+0.43±0.22	+0.24±0.32				
484.2±0.4		+0.14±0.25	-0.37±0.36				
490.2±0.5	6.0	+0.25±0.14	-0.06±0.20	6.9	^{169}Hf	$5/2^-[523]$	29/2 → 25/2
492.9	1.03×10^3	-0.02±0.03	-0.02±0.06	1.03×10^3	^{169}Hf	radioactivity	

(continued)

Table IV. cont.

E_γ (keV)	$I_\gamma^{90^\circ}$ (Arb. units)	Angular Distribution Coefficient A_2/A_o	A_4/A_o	I_γ (Arb. units)	Assignments nucleus		levels
494.9±0.6					^{169}Hf	$5/2^+[642]$	$27/2 \rightarrow 25/2$
497.6±0.2	22.8	+0.12±0.07	-0.31±0.10	24	^{169}Hf	$5/2^-[523]$	$27/2 \rightarrow 23/2$
505.4	75.5	+0.26±0.03	-0.10±0.05	87	^{169}Hf	$5/2^+[642]$	$29/2 \rightarrow 25/2$
510.9	511	+0.07±0.07	+0.10±0.11	530	e^+e^- / ^{170}Hf	0^+	$12 \rightarrow 10$
522.0		+0.17±0.07	-0.15±0.11		^{168}Hf	0^+	$10 \rightarrow 8$
528.0	36.2	+0.26±0.05	-0.07±0.08	42	^{169}Hf	$5/2^+[642]$	$27/2 \rightarrow 23/2$
531.6±0.3	9.0						
533.6±0.3	18.8	+0.24±0.23	+0.43±0.36	21			
536.0±0.2	20.8						
537.0±0.2	11.4				^{159}Tb		$5/2^+ \rightarrow 7/2^+$
543.5±0.2	9.5	+0.35±0.17	+0.08±0.24	11.5	^{169}Hf	$5/2^-[523]$	$31/2 \rightarrow 27/2$
545.5±0.2	14.3						
546.7±0.2	13.1						
550.7	20.9	+0.15±0.09	-0.29±0.14	22.6	^{170}Hf	0^+	$14 \rightarrow 12$
553.1± 0.2	11.4	+0.33±0.13	+0.01±0.19	13.7			
559.3	14.9	-0.25±0.15	-0.05±0.22	13.2	^{159}Tb		$3/2^+ \rightarrow 5/2^+$
506.9±0.3	5.1						
562.8±0.3	4.4						
568.7±0.2	12						
569.7±0.2	34	+0.20±0.04	-0.13±0.06	38	^{169}Hf	$5/2^+[642]$	$33/2 \rightarrow 29/3$
573.1±0.2	2.2						
577.1±0.5		+0.28±0.26	-0.34±0.37				

(continued)

Table IV. cont.

E_γ (keV)	I_γ 90° (Arb. units)	Angular Distribution Coefficient A_2/A_o	A_4/A_o	I_γ (Arb. units)	Assignments nucleus	bands	levels
578.3±0.2	11.6	0.00±0.35	-0.25±0.51	12			
580.7±0.2	47.8	+0.02±0.08	-0.01±0.11	48	^{159}Tb		$1/2^+ \rightarrow 3/2^+$
582.4±0.2	30.2	-0.07±0.25	+0.13±0.36	29			
584.0±0.2	29.4	-0.03±0.15	+0.22±0.22	29	^{170}Hf	0^+	16 → 14
602.7±0.2	18.8	+0.15±0.08	-0.16±0.13	20	^{169}Hf	$5/2^+[642]$	31/2 → 27/2
609.2±0.2	19.3						
612.6±0.2	6.6						
614 ±1					^{170}Hf	0^+	18 → 16
615.6±0.2	35.9	+0.01±0.23	-0.38±0.33	36	^{169}Hf	$5/2^+[642]$	37/2 → 33/2
617.1±0.3	20.8	+0.31±0.44	+0.81±0.63	25	^{159}Tb		$3/2^+ \rightarrow 3/2^+$
							$5/2^+ \rightarrow 5/2^+$
619.5±0.5	5.4						
621.3±0.3	6.8						
649.5±0.5		+0.05±0.32	-0.73±0.46		^{169}Hf	$5/2^+[642]$	41/2 → 37/2
653.5±0.5					^{170}Hf	0^+	20 → 18
663.0±0.5		+0.05±0.43	-0.54±0.61		^{169}Hf	$5/2^+[642]$	35/2 → 31/2
687 ± 2.					^{169}Hf	$5/2^+[642]$	45/2 → 41/2
706.3±0.5		+0.49±0.36	+0.02±0.48				
708 ± 2.							
718 ± 2.					(^{169}Hf	$5/2^+[642]$	49/2 → 45/2)
719.7±0.2	17.0	-0.38±0.14	-0.19±0.20	14			
727.0±0.2	6.9						

(continued)

Table IV. cont

E_γ (keV)	I_γ 90° (Arb. units)	Angular Distribution Coefficient A_2/A_o	A_4/A_o	I_γ (Arb. units)	Assignments nucleus	bands	levels
729.8±0.3	6.3						
752.8±1.0		+0.12±0.24	+0.75±0.38				
833.9±1.0		+0.22±0.18	+0.36±0.26				
836.3±1.0							
838.9±1.0							
843.2±0.5		-0.35±0.23	+0.09±0.33				
846.1±0.5							
849.0±1.0							
870.7±1.0		-0.63±0.37	-0.52±0.49				
883.9±1.0		+0.17±0.11	+0.12±0.17				
895.4±1.0		+0.30±0.16	+0.13±0.23				
911.4±0.2	16.3						
916.8±0.3	10.6						
922.5±03	5.0						
937.5±0.2	17.9	-0.17±0.19	+0.27±0.28	16			
946.8±0.2	7.3						
958.2±1.0		+0.21±0.43	+0.76±0.62				
960.0±1.0							
978.2±1.0							
983. ±0.2							
991. ±0.2							
1014.5±0.2	23.9						

(continued)

Table IV. cont.

E_γ (keV)	I_γ 90° (Arb. units)	Angular Distribution Coefficient A_2/A_o	A_4/A_o	I_γ (Arb. units)	Assignments nucleus	bands	levels
1116.1±0.3	10.1						
1121.3±0.3	65.3						
1173.3±0.6	14.3						
1189.1±0.3	25.8						
1220.1±1.1	23.4						
1221.9±0.5	36.7						

Angle-integrated photon relative intensity estimated by dividing column 2 by 1 - $A_2/2A_0$. Values of A_4/A_0 were felt to be too uncertain to include in correction.

Table V. Coincidences from the reaction $^{159}Tb(^{14}N,4n\gamma)^{169}Hf$.

Gate (keV)	Coincident γ lines (keV)[a]
28.8[b]	107.8, 207.1, 218,6, (278.5), 326.3, 330.8, 423.4, (437.9)
58.1	K_x(Tb), 79.5, 103.9, 121.1, 183.4
67.3	166.5, 207.1, 218.6, (326.3), (423.4)
79.5	K_x(Tb), 58.1, 103.9, 121.1, 148.4, 225.0, 269.4, (307.1)
86.4	K_x(Tb-Dy,(Yb)), 79.5, (121.1), 197, 297, 386
99.6	K_x((Tb,Hf), 77.8, 130.0, (154.1), (179.3), (198.3), 220.9, 320.7
100.8	220.9, 320.7, 400.3, 462.1, 551
103.9	K_x(Tb), 58.1, 79.5, (88), 121.1, 137.5, 148.4, 269.4
107.8	166.5, 218.6, (278.5), 326.3, 330.8, (390), 423.4, (437.5), (497.6), (505.4), (570)
121.1	K_x(Tb), 58.1, 79.5, 103.9, 137.5, 148.4, 183.4, 371.2
123.7	K_x(Lu,Hf), 261.7, (316.1), 369.4, 371.4, 371.2, 456.8, 511
130.0	K_x(Hf), 59.1, 99.6, 154.1, (179.3), (198.3), (265.0), (333.2), (1406.3)
137.5	K_x(Tb), (99.6), 103.9, 121.1, (130), 225.0
146.8	K_x(Tb,Hf), 164.8, (198.3), 709.7
148.4	K_x(Tb), 58.1, 79.5, 103.9, 121.1, 225.0, 269
154.1	K_x(Hf), (99.6), 130.0, (159), (179.3), 290.5, (377.6)
158.9	K_x(Tb), 79.5, 103.9, 148.4
164.8	K_x(Hf), (99.6), 146.8, 182.0, (381)
166.5	40, K_x(Hf), 67.3, 107.8, 326.3, 330.8, 437.9, (505.4), (528.0)
177.1	267.1, 346.2, 411.2, (490.2)

(continued)

Table V cont.

Gate (keV)	Coincident γ lines (keV)[a]
179.3	K_x(Hf), (99.6), 130.0, 146.8, 154.1, (198.3)
182.0	K_x(Tb), 121.1, 164.8,
183.4	K_x(Tb), 58.1, 121.1, 148.4
197.0	K_x(Dy), 86.4, 297.2, 386.2, (443)
198.3	K_x(Yb), 87.4, 146.8, 296, (385)
207.1	K_x(Hf), 67.3, (73.2), (326.3), 330.8, 423.4, 437.9, (528.0), (602.7)
218.6	40, K_x(Hf), 67.3, 107.8, 278.5, 326.3, 390.3, 423.4, 505.4, 569.7, 615.6
220.9	K_x(Hf), 100.8, 320.7, 400.3, 462.1, 511, 550.7
225.0	K_x(Tb,(Hf)), 58.1, 77.8, 79.5, (148.4), 311.2, 384.5, 445.2, (497.6)
227.9	K_x(Yb), 102.4, 337.5, (430.1)
261.7	K_x(Hf), 123.7, 371.2
267.1	K_x(Hf), 99.6, 148.4, 177.1, (214), (311), 346.2, 411.2, 460.6, 490.2, 553.1, 584.0
269.4	K_x(Tb), 79.5, 103.9, 157.2, (183)
278.5	K_x(Hf), 107.8, 166.5, (207.1), 218.6, 437.9
307.2	K_x(Tb,(Hf)), 121.1, (400), (462)
311.2	K_x(Hf), (77.8), 225.0, 384.5, 445.2
320.7	K_x(Hf), 100.8, 220.9, 400.3, 462.1, 511, 550.7, (584)
326.3	(40), K_x(Hf), (52), 67.3 , 107.8, 207.1, 218.6, (390.3), 423.4, 505.4, 569.7, (615.6)

(continued)

Table V. cont.

Gate (keV)	Coincident γ lines (keV)[a]
330.8	(40), K_x(Tb,Hf), (67.3), (103.9), 166.5, 207.1, (220.9), 437.9, 528.0, 602.7
333.4	K_x(Hf), (130.0)
337.5	K_x(Yb), 102.4, 227.9, (430.1)
346.2	K_x(Hf), (140), (148), 177.1, 267.1, (340.0), 411.2, (445.2), 460.6, 490.2
363.4	K_x(Tb), 184.4
369.4	K_x(Lu), 123.7, 511
371.2	K_x(Hf), 123.7, 261.7, 456.8
377.6	K_x(Hf), (99.6), (130.0), (154.1), (284.1)
384.5	K_x(Hf), (148.4), 225.0, (267.1), (278.5), 311.2, 445.2, 497.6
386.2	86.4, 197.0, 297.2
390.3	K_x(Hf), 166.5, 218.6, 326.3, (346)
400.3	K_x(Hf), 100.8, 220.9, 320.7, 462.1, 511, 550.7, (594)
411.2	K_x(Hf), (86.4), (148.4), (166.5), 177.1, 207.1, 267.1, 346.2, 460.6, (490.2)
423.4	K_x(Hf), 107.8, (164.8), 207.1, 218.6, 326.3, 505.4, 569.7
430.1	(102.4), 227.9, 337.5
437.9	K_x(Hf), (67.3), 107.8, 166.5, 207.1, 218.6, 278.5, 330.8, (381.2), 528.0, 602.6
445.2	K_x(Hf), 225.0, 311.2, 384.5, 497.6, 543.5
460.6	K_x(Hf), 100, 220.9, 267.1, 320.7, 346.2, 411.2, 490.2

(continued)

Table V. cont.

Gate (keV)	Coincident γ lines (keV)[a]
462.1	K_X(Hf), 100, 220.9, 320.7, 400.3, 5.11, 584.0
492.9	K_X(Lu), 511
497.6	K_X(Hf), 311.2, (384.5), (445.2)
505.4	K_X(Hf), 311.2, (384.5), (445.2)
505.4	K_X(Hf), 107.8, 218.6, 326.3, 423.4, 569.7, (615.6)
528.0	K_X(Hf), (107.8), 166.5, 207.1, 218.6, 278.5, 330.8, 437.9
550.7	K_X(Hf), 100, 220.9, 320.7, 400.3, 462.1, 511
569.7	K_X(Hf), 218.6, 326.3, 423.4
584.0	K_X(Hf), (220.9), 320.7, 400.3, (511), (550.7)
602.7	K_X(Hf), (207.1), (218.6), 278.5), (330.8), (437.9)
615.6	(K_X(Hf)), 218.6, (320.7), 326.3, 423.4, 462.1, (505.7), (550.7), 569.7, (584.0)

[a] Weak, or marginal coincidences are shown in parentheses.

[b] 28.8 keV gate in the STOP detector; only events where the STOP signal occurred 50 - 150 ns after the maximum of the "prompt" peak were accepted.

Table VI. Added Coincidences in ^{169}Hf with Transitions of Established Bands

Band	Gates (keV)	Coincident γ lines (keV)
$5/2^+[642]$ [a]	218.6+326.3+423.4+505.4+569+615.6	KX(Hf), 67.3, 107.8, 166.5, 207.1, 218.6, 278.5, 326.3, 390.3,423.4, (495), 505.4, (514), 569.7, 615.6, 650, (689)
$5/2^+[642]$ [b]	166.5+207.1+330.8+437.9+528.0+602.7	KX(Hf), 67.3, 107.8, 166.5, 207.1, (218.6), 278.5, 326.3, 330.8, (369.4), (423.4), 437.9, 505.4, 528.0, 602.7
$5/2^-[523]$ [a]	267.1+346.2+411.2+460.6	KX(Hf), 77.8, 99.6, (139.6), 148.4, 177.1, 267.1, (311.2), 346.2, 411.2, 460.6, 490.2, (514)
$5/2^-[523]$ [b]	311.2+384.5+445.2+497.6	KX(Hf), 77.8, (197), 225.0, 265.0, 311.2, 384.5, 445.4, 497.6, 543.5
$5/2^-[512]$	130.0+154.1+179.3+284.1+377.6	KX(Hf), 59.1, 99.6, (102.4), 130.0, 154.1, 158.9, 198.3, (265.0), (267.1), 377.6, 406.3, (436.1)

[a] I + 1/2 odd.

[b] I + 1/2 even.

Table VII. Rotational parameters of the $5/2^-[523]$ and $5/2^-[512]$ bands in ^{169}Hf.

Band	A(keV)	B(eV)	A_{2k}(meV)
$5/2^-[523]$	11.66 ± 0.03	-6.61 ± 0.12	38.5 ± 1.7
$5/2^-[512]$	14.78 ± 0.12	-12.4 ± 1.7	-55 ± 42

Table VIII. Mixing amplitudes and g-factors in negative parity bands of ^{169}Hf.

Band	Initial Spin	Mixing Amplitudes			$(g_K-g_R)_{exp.}$	$(g_K-g_R)^a_{th.}$
		from angular distribution	from branching ratio	adopted value		
$5/2^-[523]$	9/2		$\pm 0.70 \pm 0.21$[b]	-0.70 ± 0.21	-0.13 ± 0.04	-0.12
$5/2^-[512]$	9/2	-4.0 to -0.05	$\pm 0.35 \pm 0.10$	-0.35 ± 0.10	-0.47 ± 0.15	-0.62
	11/2	-6.0 to -0.03	$\pm 0.22 \pm 0.07$	-0.22 ± 0.07	-0.66 ± 0.22	-0.62
	13/2	-10 to +0.02	$\pm 0.18 \pm 0.05$	-0.18 ± 0.05	-0.79 ± 0.26	-0.62

[a] Values of g_K extrapolated from ref. 27, and $g_R = -0.3$ were used.

[b] From analysis of coincidence spectra.

FIGURE CAPTIONS

Fig. 1. Low energy γ- and X-ray spectrum of ^{169}Ta taken during three consecutive time intervals following the end of irradiation. The measurement intervals are shown in the figure as minutes:seconds.

Fig. 2. Partial decay scheme of ^{169}Ta.

Fig. 3. Single γ-ray spectrum produced by 68 MeV ^{14}N ions in Tb target. The ^{169}Hf band assignments are shown by arrows and I_i values; asterisks * indicate $I_i \rightarrow I_i - 1$ transitions, the rest the $I_i \rightarrow I_i - 2$ lines. Transitions are indicated by band as follows: A, $5/2^-[523]$; A', 170 Hf Ground Band; B, ^{159}Tb Target Ground Band Transitions excited by inelastic scattering; C, $5/2^-[512]$; D, $5/2^+[642]$.

Fig. 4. Delayed time spectrum connected with the 28.8 keV level (open circles) and "prompt" time spectrum corresponding to nearly the same energy windows (solid dots).

Fig. 5. Coincidence spectra added for the two cascades in $5/2^+[642]$ band; I + 1/2 odd in upper part, I + 1/2 even in lower part of the figure.

Fig. 6. ^{169}Hf level scheme based on this study.

Fig. 7. Three-parameter fit of the $5/2^-[523]$ band.

Fig. 8. Systematics of the rotational parameter $\hbar^2/2\mathcal{J}$ of the $5/2^-[512]$ band for N = 97 and for Z = 72 (Hf).

Fig. 9. Comparison of the $g_K - g_R$ values for the two considered assignments of the band at 59.1 keV with the theoretical predictions.[27] The values determined for the $3/2^-[521]$ assignment are shown in the left part (open circles), for the $5/2^-[512]$ assignment in the right part of the figure (solid circles). The heavy line is the theoretical value.

Fig. 10. Dependence of the moments of inertia on nuclear rotation in ^{169}Hf and ^{168}Hf. See text for the discussion of quantum number R.

Fig. 11. Determination of the mixing amplitudes for the 166.5 keV, $15/2^+ \rightarrow 13/2^+$ transition in the $5/2^+[642]$ band.

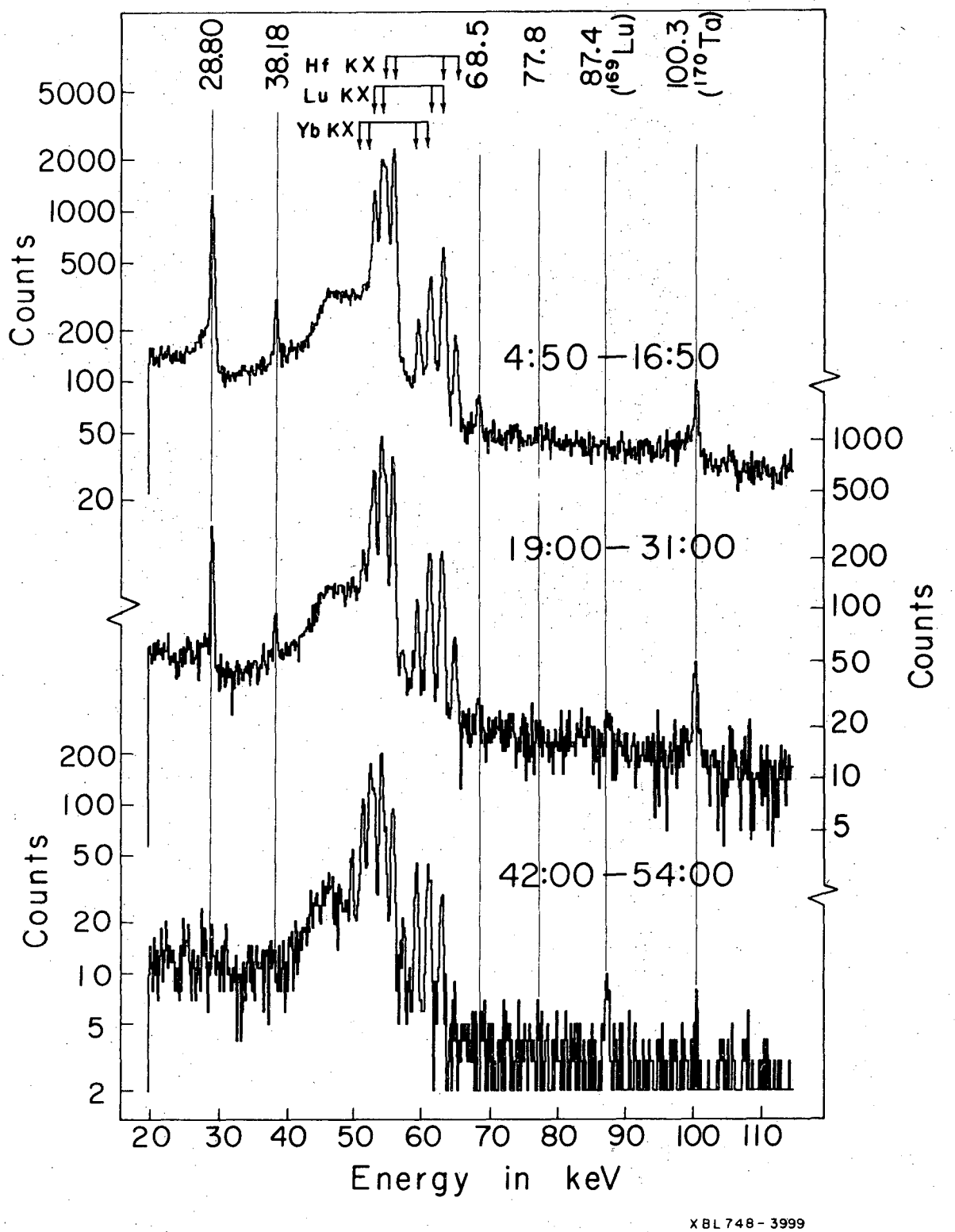
28.80
38.18
Hf KX
Lu KX
Yb KX
68.5
77.8
87.4
(169Lu)
100.3
(170Ta)
4:50 — 16:50
19:00 — 31:00
42:00 — 54:00
Counts
Counts
Counts
Energy in keV
XBL 748-3999

Fig. 1

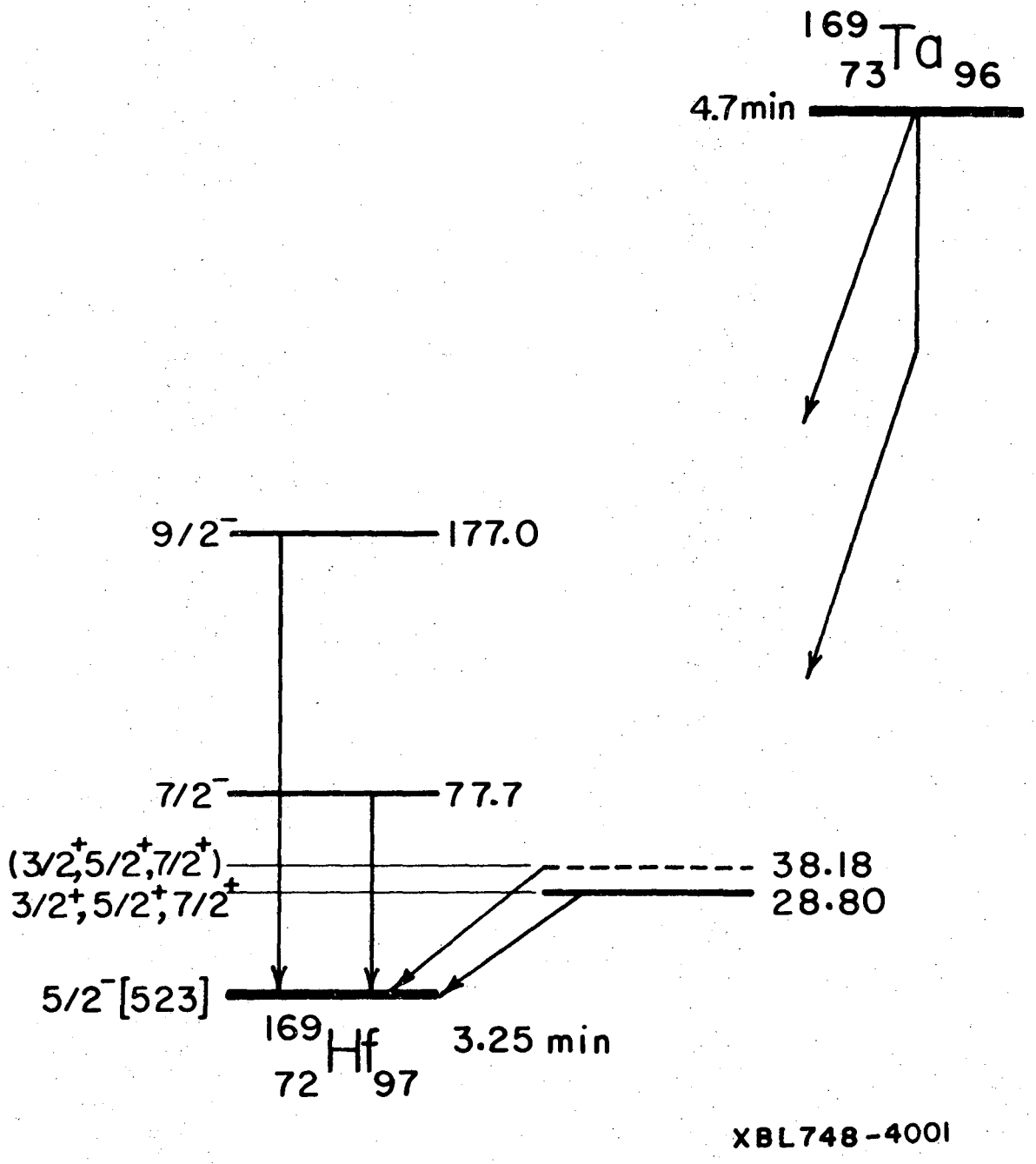
169 73 Ta 96
4.7min
9/2⁻
177.0
7/2⁻
77.7
(3/2⁺,5/2⁺,7/2⁺)
3/2⁺,5/2⁺,7/2⁺
38.18
28.80
5/2⁻[523]
169 72 Hf 97
3.25 min
XBL748-4001

Fig. 2

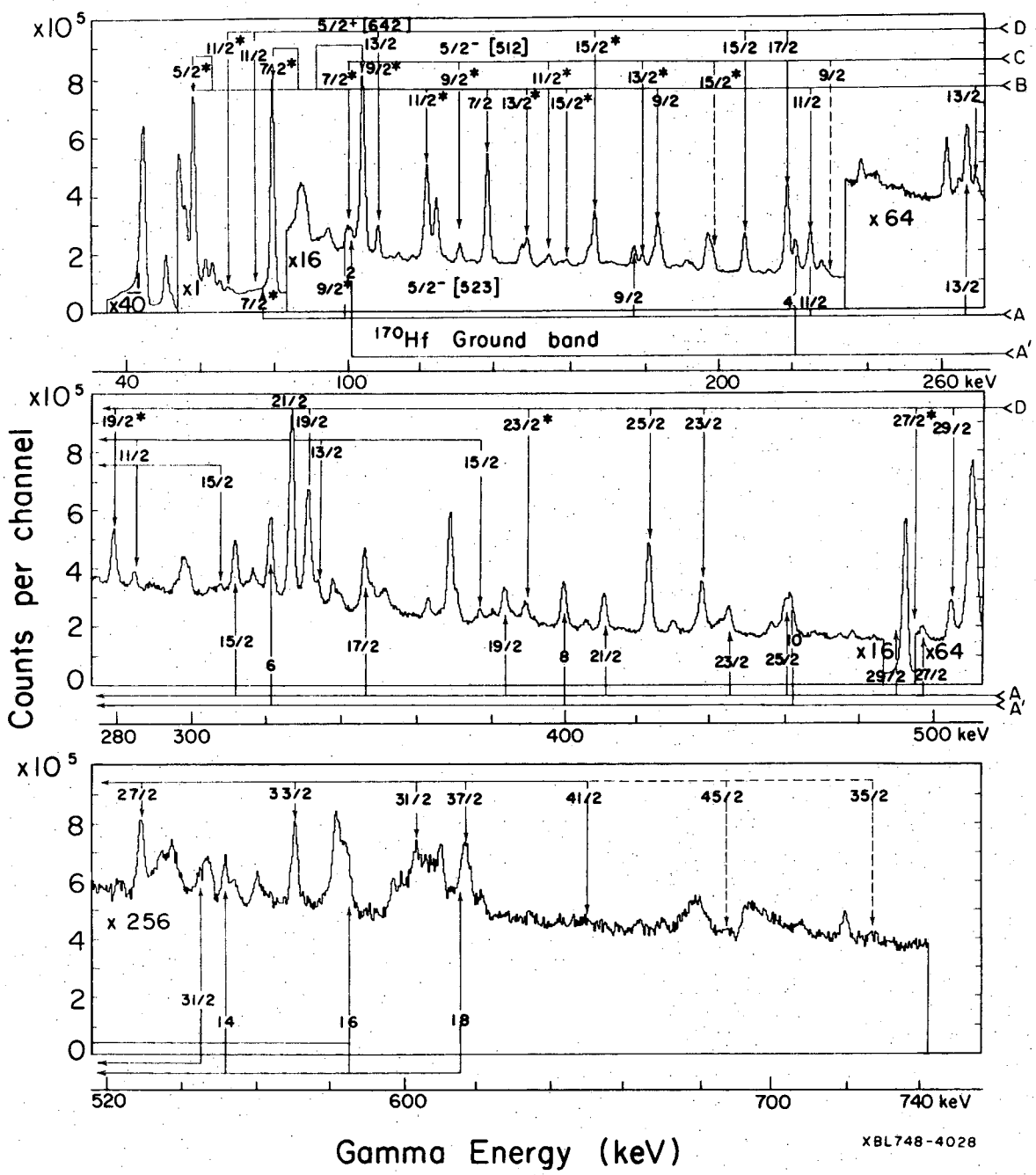
Counts per channel
Gamma Energy (keV)
^{170}Hf Ground band
5/2+ [642]
5/2- [512]
5/2- [523]
x64
x16
x40
x256
XBL748-4028

Fig. 3

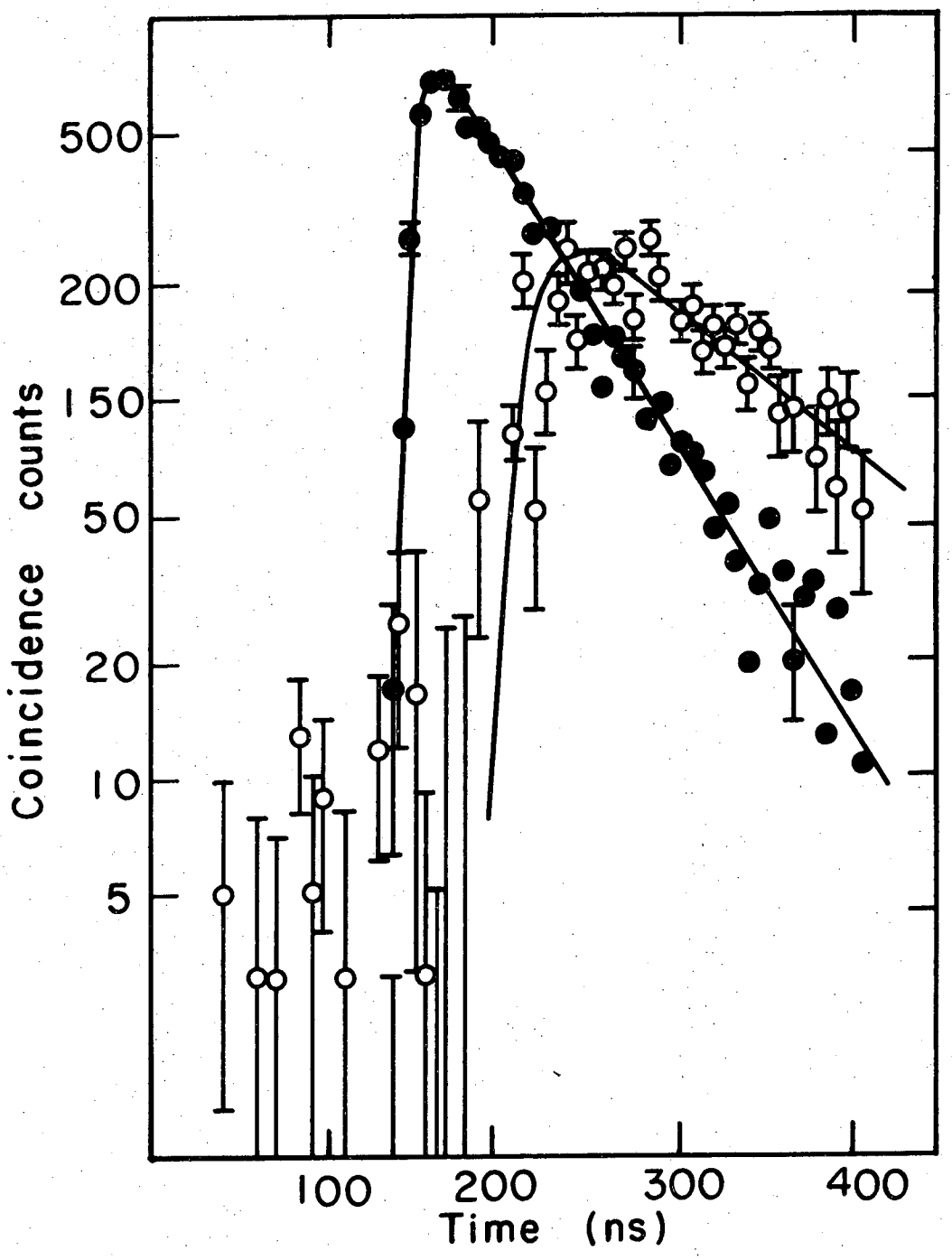
500
200
150
50
20
10
5
Coincidence counts
100
200
300
400
Time (ns)
XBL746-3468

Fig. 4

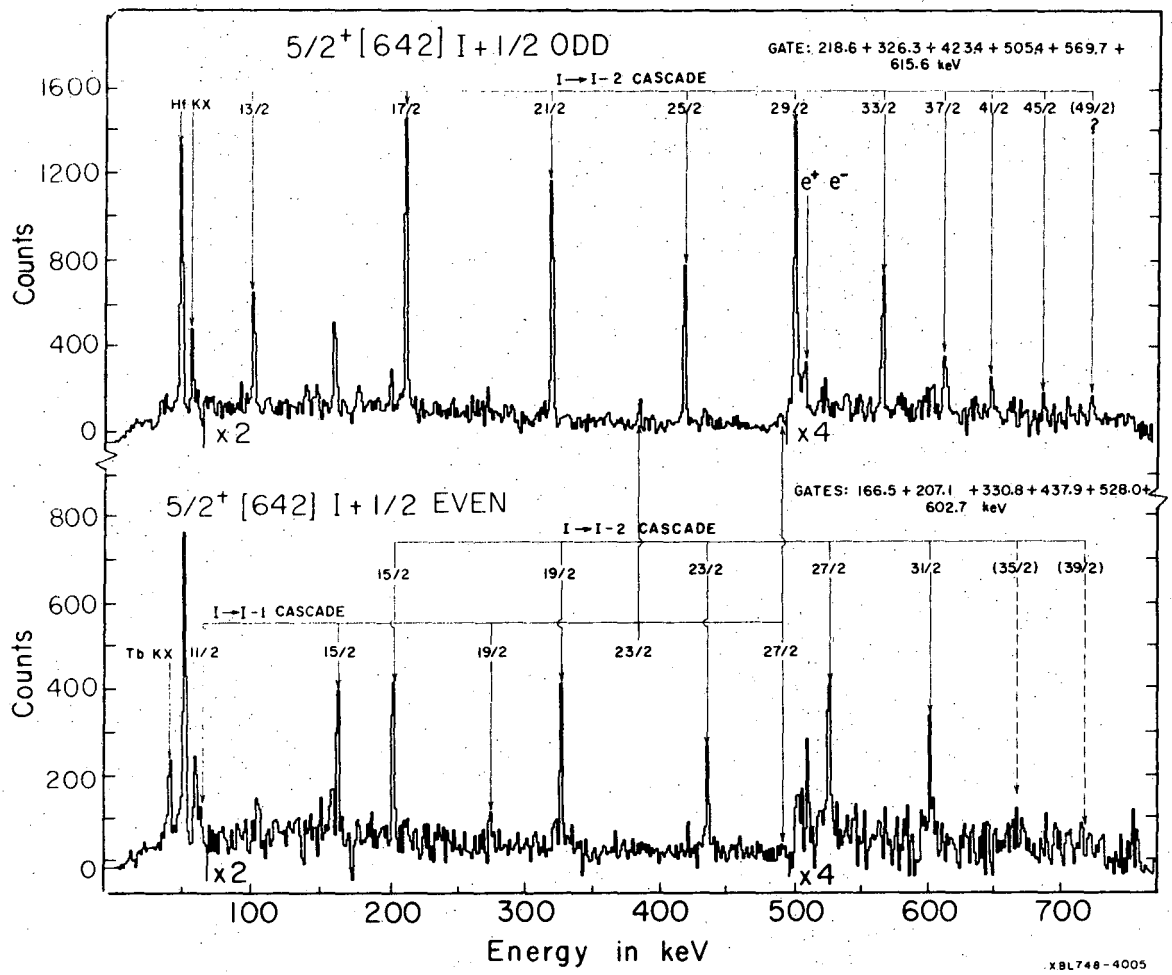
5/2+[642] I+1/2 ODD
GATE: 218.6 + 326.3 + 423.4 + 505.4 + 569.7 + 615.6 keV
I→I-2 CASCADE
Hf KX
13/2
17/2
21/2
25/2
29/2
33/2
37/2
41/2
45/2
(49/2)
?
e+ e-
x2
x4
5/2+ [642] I+1/2 EVEN
GATES: 166.5 + 207.1 + 330.8 + 437.9 + 528.0 + 602.7 keV
I→I-2 CASCADE
15/2
19/2
23/2
27/2
31/2
(35/2)
(39/2)
I→I-1 CASCADE
Tb KX
11/2
15/2
19/2
23/2
27/2
x2
x4
Counts
Energy in keV
XBL748-4005

Fig. 5

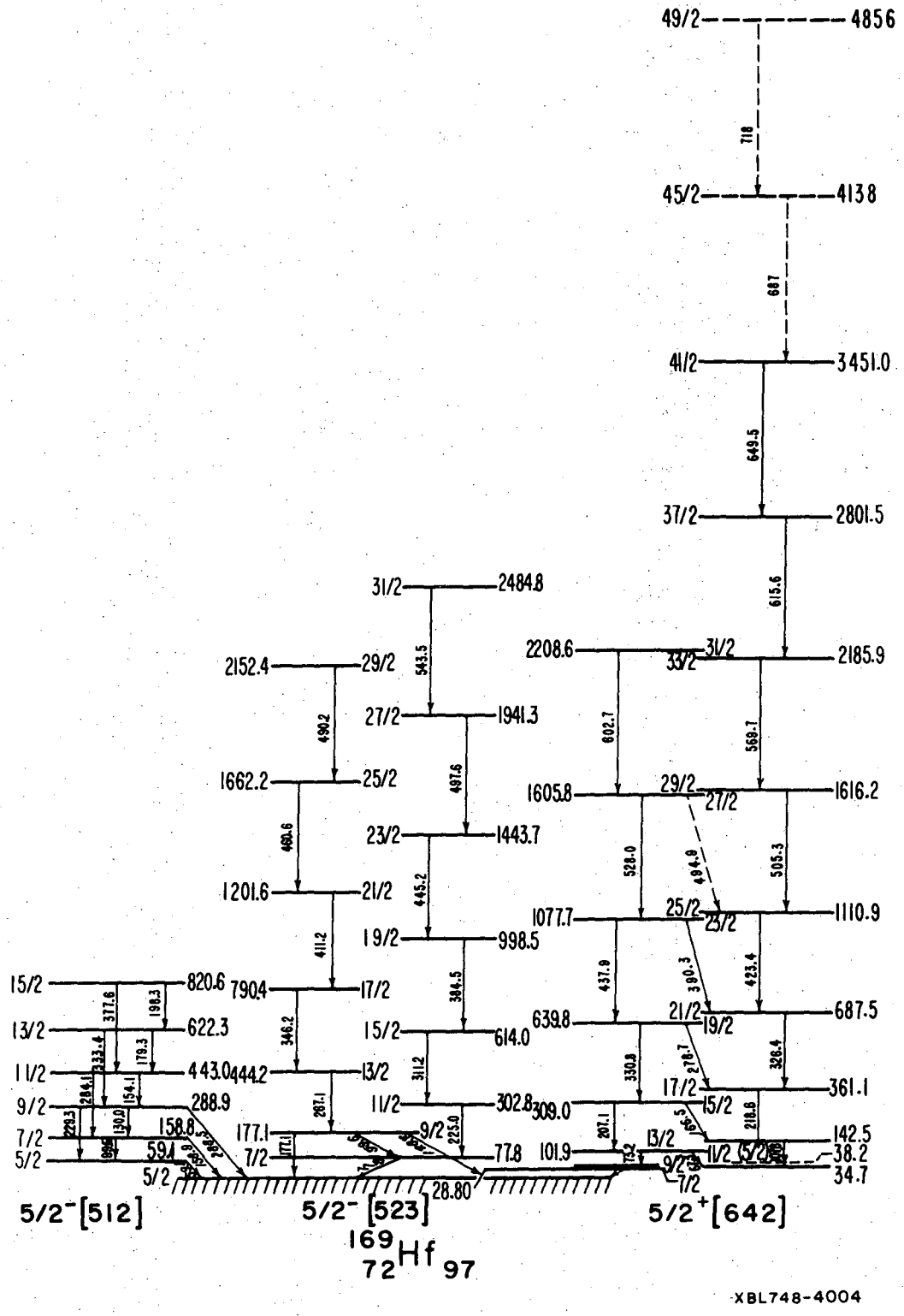
49/2
4856
718
45/2
4138
687
41/2
3451.0
649.5
37/2
2801.5
615.6
31/2
2484.8
2208.6
33/2
31/2
2185.9
2152.4
29/2
543.5
602.7
568.7
27/2
1941.3
490.2
1662.2
25/2
497.6
1605.8
29/2
27/2
1616.2
460.6
23/2
1443.7
528.0
494.9
505.3
1201.6
21/2
445.2
1077.7
25/2
23/2
1110.9
411.2
19/2
998.5
437.9
390.3
423.4
15/2
820.6
790.4
17/2
384.5
639.8
21/2
19/2
687.5
377.6
198.3
346.2
13/2
622.3
15/2
614.0
333.4
179.3
330.8
278.7
326.4
11/2
443.0
444.2
13/2
311.2
17/2
15/2
361.1
284.1
154.1
9/2
288.9
11/2
302.8
309.0
287.1
223.0
218.8
220.3
130.0
158.8
177.1
9/2
65.5
7/2
59.4
177.1
7/2
77.8
101.9
13/2
11/2
5/2
142.5
38.2
34.7
5/2
28.80
9/2
7/2
5/2⁻[512]
5/2⁻[523]
5/2⁺[642]
169
72Hf97
XBL748-4004

Fig. 6

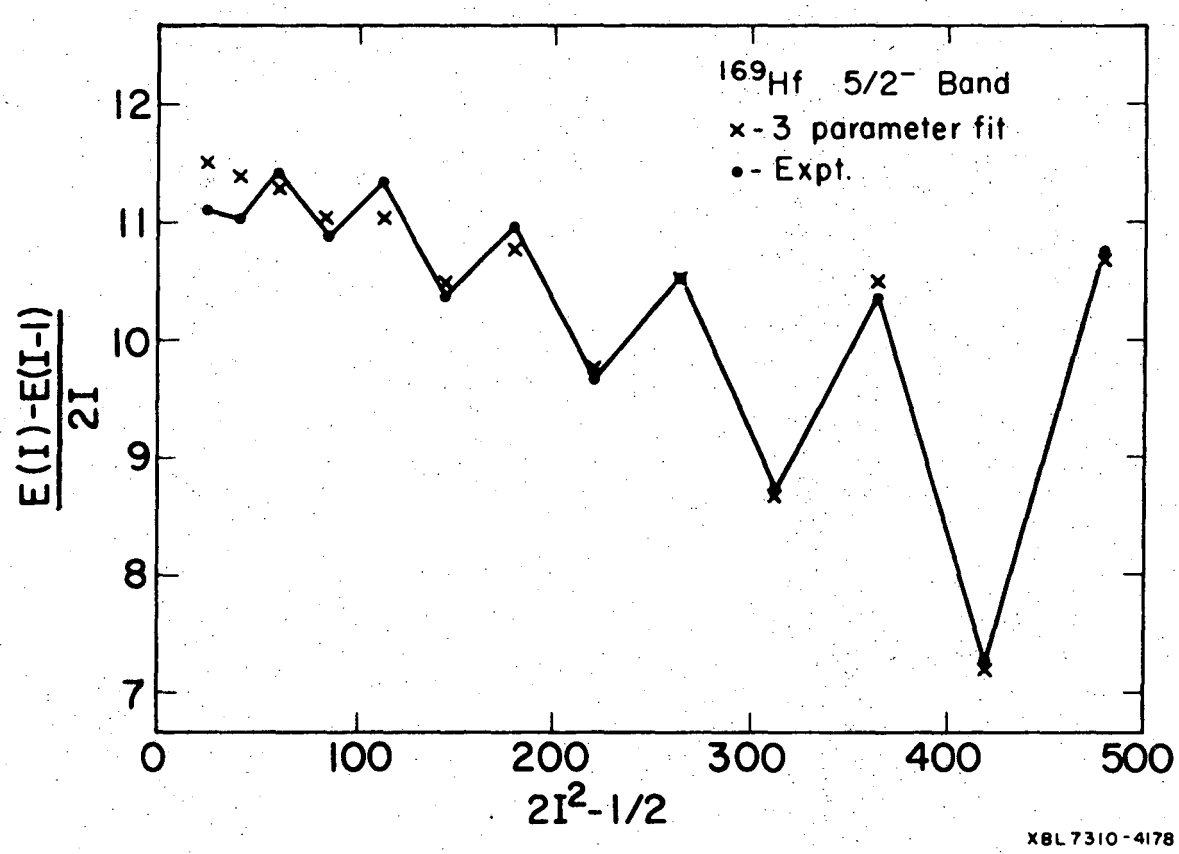
^{169}Hf 5/2$^-$ Band
× - 3 parameter fit
• - Expt.
$\frac{E(I)-E(I-1)}{2I}$
12
11
10
9
8
7
0
100
200
300
400
500
$2I^2-1/2$
XBL7310-4178

Fig. 7

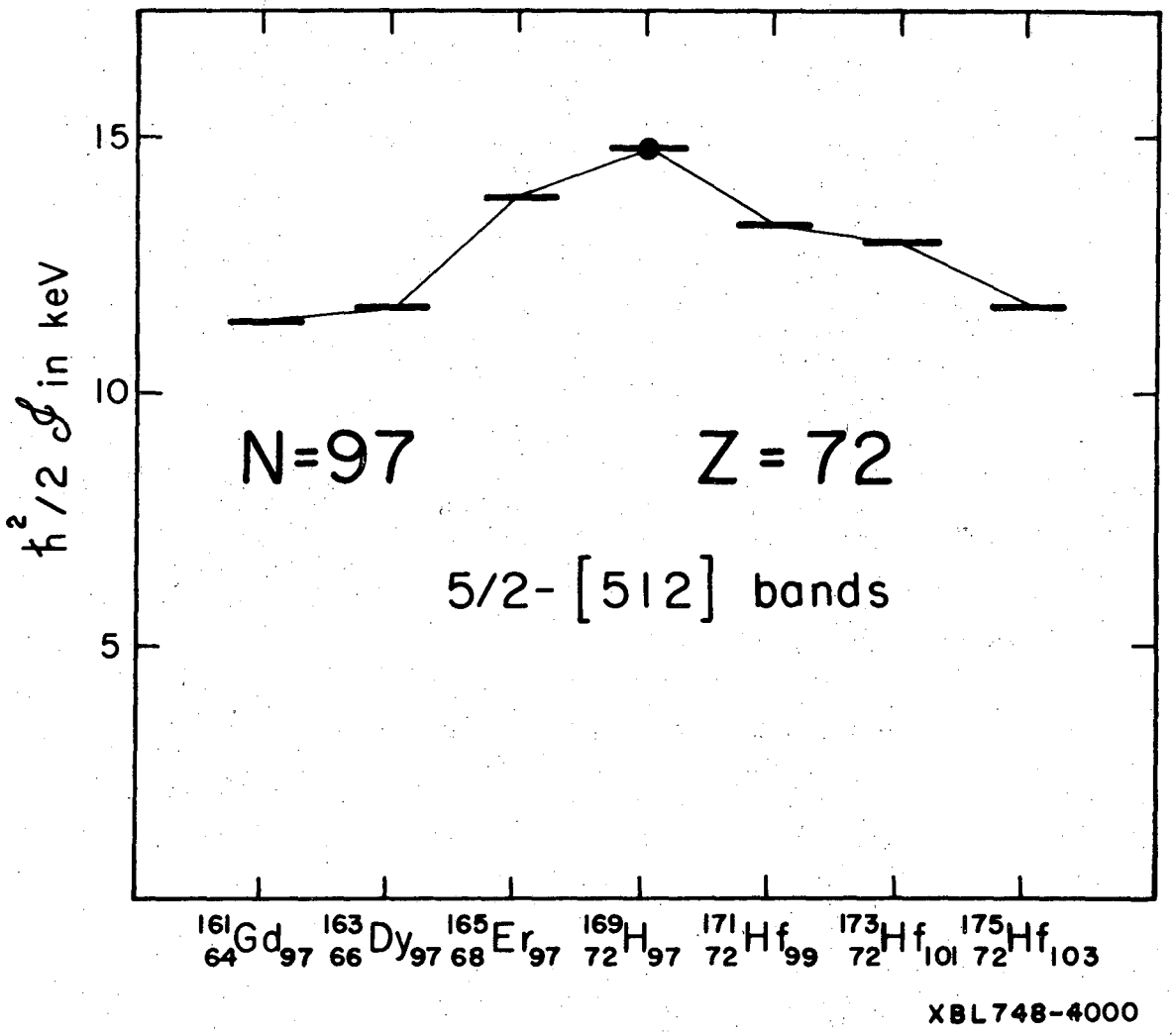
15
10
5
$\hbar^2/2\mathcal{J}$ in keV
N=97
Z=72
5/2-[512] bands
$^{161}_{64}Gd_{97}$ $^{163}_{66}Dy_{97}$ $^{165}_{68}Er_{97}$ $^{169}_{72}H_{97}$ $^{171}_{72}Hf_{99}$ $^{173}_{72}Hf_{101}$ $^{175}_{72}Hf_{103}$
XBL748-4000

Fig. 8

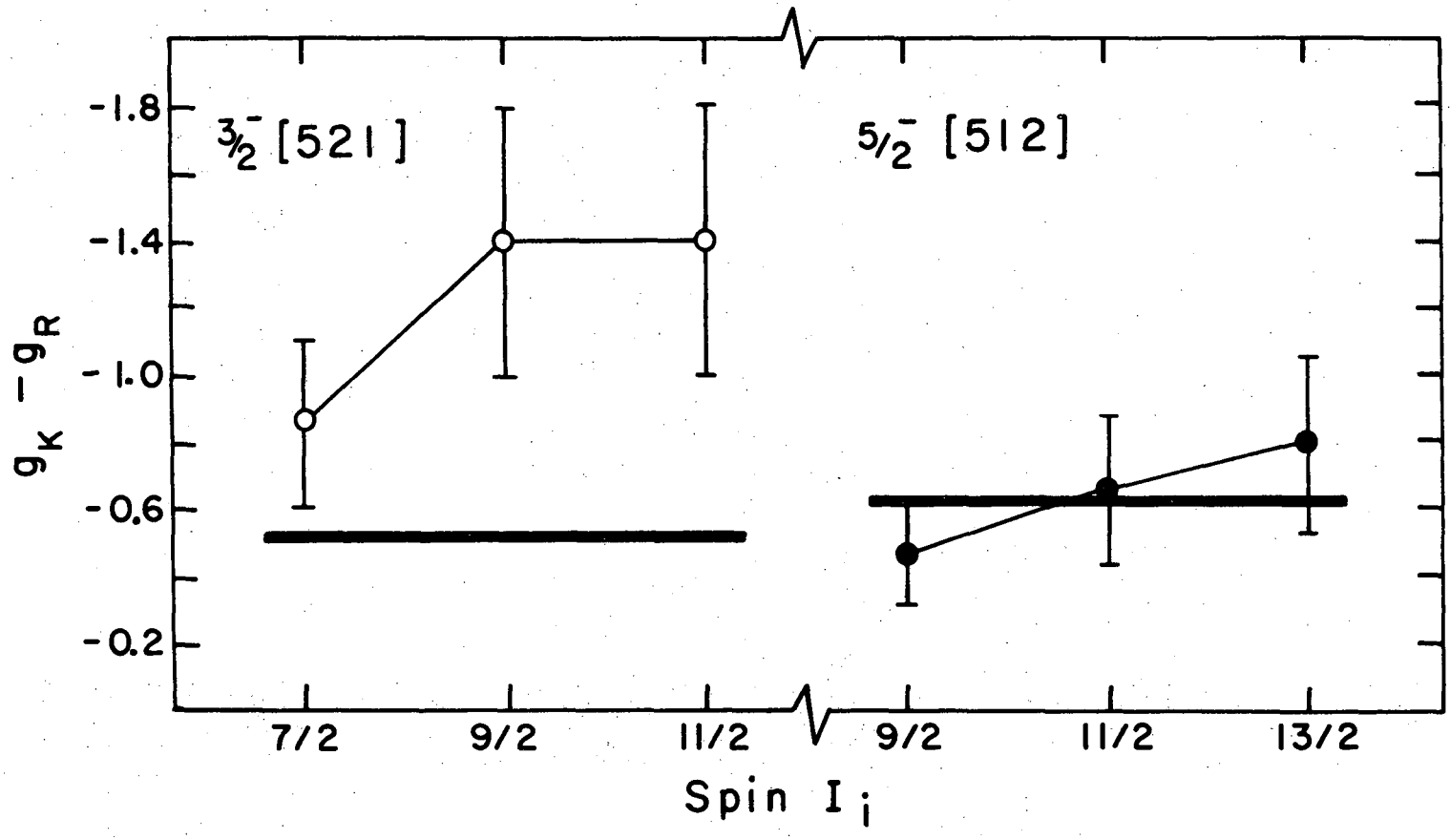

XBL747-4003

Fig. 9

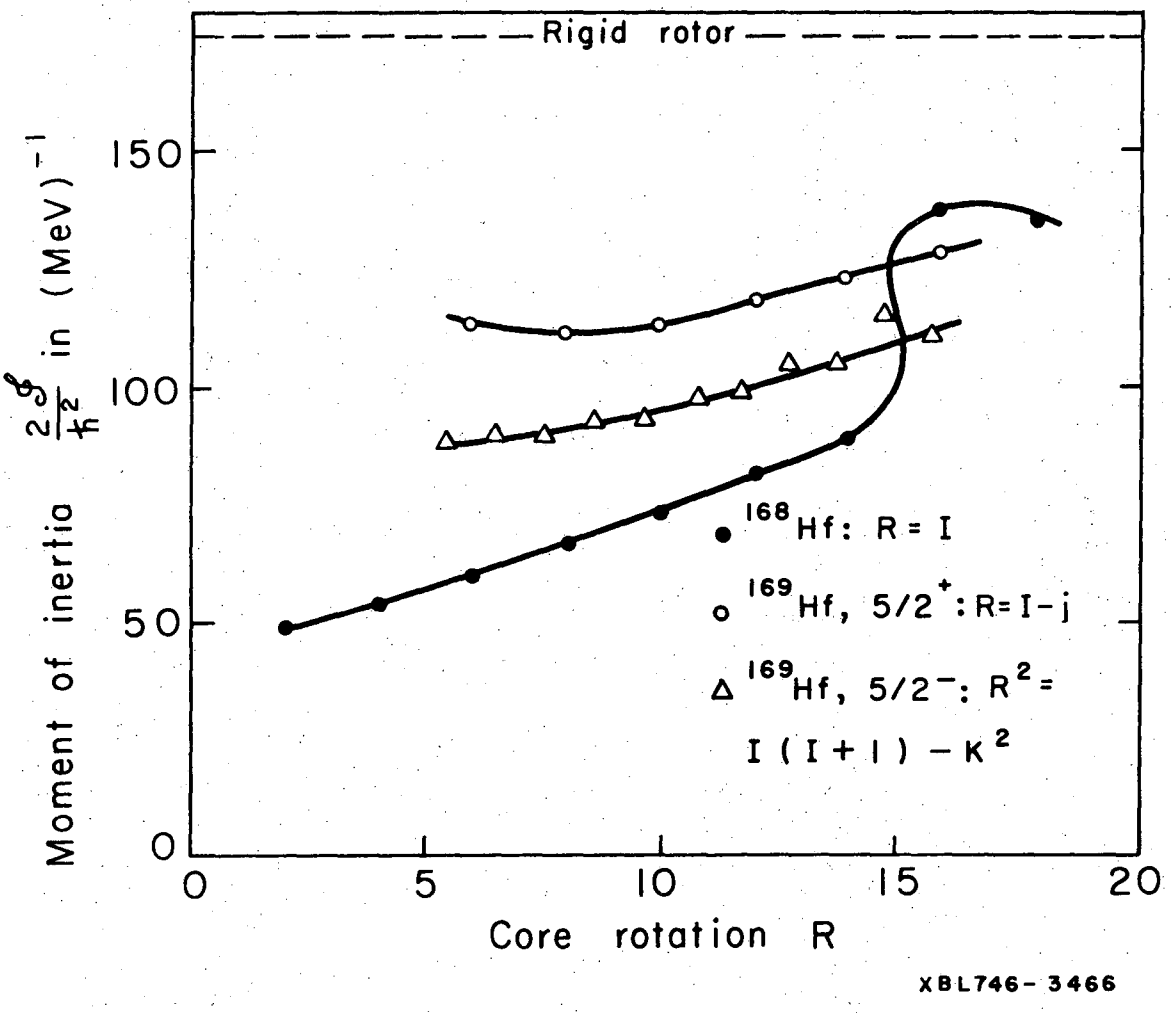
Rigid rotor
Moment of inertia $\frac{2\mathcal{J}}{\hbar^2}$ in $(MeV)^{-1}$
150
100
50
0
0
5
10
15
20
Core rotation R
^{168}Hf: R = I
^{169}Hf, 5/2$^+$: R=I-j
^{169}Hf, 5/2$^-$: R^2 = I(I+1) − K^2
XBL746-3466

Fig. 10

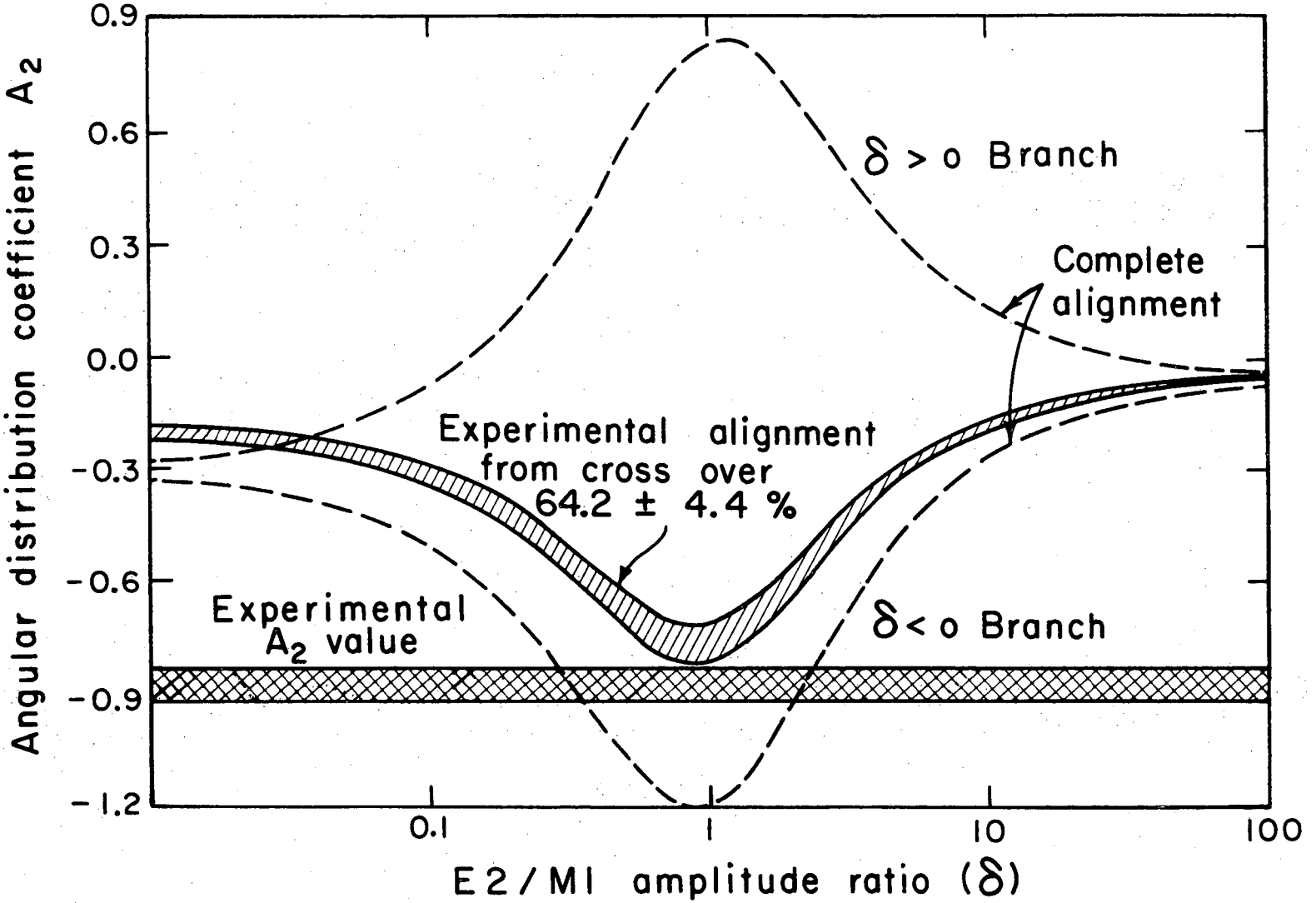
0.9
0.6
0.3
0.0
-0.3
-0.6
-0.9
-1.2
Angular distribution coefficient A_2
δ > o Branch
Complete alignment
Experimental alignment from cross over 64.2 ± 4.4 %
Experimental A_2 value
δ < o Branch
0.1
1
10
100
E2 / M1 amplitude ratio (δ)
XBL746-3470

Fig. 11

LEGAL NOTICE

This report was prepared as an account of work sponsored by the United States Government. Neither the United States nor the United States Atomic Energy Commission, nor any of their employees, nor any of their contractors, subcontractors, or their employees, makes any warranty, express or implied, or assumes any legal liability or responsibility for the accuracy, completeness or usefulness of any information, apparatus, product or process disclosed, or represents that its use would not infringe privately owned rights.

TECHNICAL INFORMATION DIVISION
LAWRENCE BERKELEY LABORATORY
UNIVERSITY OF CALIFORNIA
BERKELEY, CALIFORNIA 94720